The organic sea surface microlayer in the upwelling region off Peru and potential implications for air-sea exchange processes

Anja Engel* and Luisa Galgani

GEOMAR – Helmholtz Centre for Ocean Research Kiel, Düsternbrooker Weg 20, 24105 Kiel, Germany

* aengel@geomar.de

Abstract: The sea surface microlayer (SML) is at the very surface of the ocean, linking the hydrosphere with the atmosphere. The presence and enrichment of organic compounds in the SML have been suggested to influence air-sea gas exchange processes as well as the emission of primary organic aerosols. Here, we report on organic matter components collected from an approximately 50µm thick SML and from the underlying water (ULW), ~20 cm below the SML, in December 2012 during the SOPRAN METEOR 91 cruise to the highly productive, coastal upwelling regime off Peru. Samples were collected at 37 stations including coastal upwelling sites and off-shore stations with less organic matter and were analyzed for total and dissolved high molecular weight (>1kDa) combined carbohydrates (TCCHO, DCCHO), free amino acids (FAA), total and dissolved hydrolysable amino acids (THAA, DHAA), transparent exopolymer particles (TEP), Coomassie stainable particles (CSP), total and dissolved organic carbon (TOC, DOC), total and dissolved nitrogen (TN, TDN), as well as bacterial and phytoplankton abundance. Our results showed a close coupling between organic matter concentrations in the water column and in the SML for almost all components except for FAA and DHAA that showed highest enrichment in the SML on average. Accumulation of gel particles, i.e. TEP and CSP, in the SML differed spatially. While CSP abundance in the SML was not related to wind speed, TEP abundance decreased with wind speed, leading to a depletion of TEP in the SML at about 5 m s^{-1}. Our study provides insight to the physical and biological control of organic matter enrichment in the SML, and discusses the potential role of organic matter in the SML for air-sea exchange processes.

1. Introduction

The sea-surface microlayer (SML) is the uppermost layer of the water-column and the interface between the ocean and the atmosphere. The accumulation of organic matter, distinct physical and chemical properties and a specific organismal community (neuston) distinguish the SML as a unique biogeochemical and ecological system. It has been suggested that the SML has a gel-like nature (Cunliffe and Murrell, 2009; Sieburth, 1983) of varying thickness (20-150 µm, Cunliffe et al., 2013) with dissolved polymeric carbohydrates and amino acids present as well as gel particles, such as transparent exopolymer particles (TEP) of polysaccharidic composition, and Coomassie stainable particles (CSP) of proteinaceous composition. These gelatinous compounds originate from high molecular weight polymers that are released form phytoplankton and bacterial cells by exudation and cell break up (Chin et al., 1998; Engel et al., 2004; Verdugo et al., 2004). Polysaccharide-rich gels, like TEP, were attributed mainly to phytoplankton exudation (Passow, 2002), while the production of protein-containing gels, such as CSP, has been related to cell lysis and decomposition, as well as to the absorption of proteins onto non-proteinaceous particles (Long and Azam, 1996). Gels are transported to the SML by rising bubbles (Azetsu-Scott and Passow, 2004; Zhou et al., 1998) or are produced from dissolved precursors directly at the air-sea interface during surface wave action (Wurl et al., 2011). Gel particles can promote microbial biofilm formation (Bar-Zeev et al., 2012) and mediate vertical organic matter transport, either to the atmosphere (Leck and Bigg, 2005; Orellana et al., 2011) or to the deep ocean (Passow, 2002).

Accumulation of organic matter in the SML may be tightly coupled to phytoplankton abundance in the water-column (Bigg et al., 2004; Galgani et al., 2014; Gao et al., 2012; Matrai et al., 2008).

Thus, organic matter accumulation and composition in the SML may also reflect the sensitivity of marine microorganisms in the surface ocean to environmental changes, which was shown during previous mesocosms studies (Engel et al., 2013; Riebesell et al., 2009; Schulz et al., 2013). Distinct from the SML and on top of it lies the nanolayer, a monomolecular film, which, like the SML, shows seasonality features with carbohydrate-rich polymeric material being most abundant during the summer months and possibly related to a combination of primary production (phytoplankton abundance) and photochemical and/or microbial reworking of organic matter (Laß et al., 2013).

In our study we focused on the upper micrometers of the water-air interface that we operationally define as SML, whose compositional changes and accumulation of organic matter may influence two air-sea interface processes necessary to understand oceanic feedbacks on the atmosphere: sea-spray aerosol (SSA) emission and air-sea gas exchange (Cunliffe et al., 2013). During biologically productive periods, a high amount of SSA with a predominant organic composition is emitted from the ocean's surface (O'Dowd et al., 2004). These compounds primarily reveal a polysaccharidic, gel-like composition, suggesting that the abundance and size of dissolved polysaccharides and marine gels in the sea surface may influence the organic fraction of SSA (Orellana et al., 2011; Russell et al., 2010). It has also been shown that the presence of biogenic surface active substances (surfactants) in the SML leads to capillary wave damping, alters the molecular diffusion of gases (Frew et al., 1990; Liss and Duce, 2005) and therewith affects gas exchange rates particularly at lower wind speed (Jähne and Haußecker, 1998). In this respect, the understanding of sources, composition and fate of biological components in the SML becomes of particular relevance for environments, where biological productivity is high like in coastal upwelling regimes.

Off Peru, the coastal upwelling region extends between approximately 4°S and 40°S. In this area, upwelling processes are sustained by winds throughout the year but feature high inter-annual variability induced by the El Niño-Southern Oscillation (ENSO) cycle (Tarazona and Arntz, 2001). Eastern Boundary Upwelling Systems (EBUS's) like the system off Peru are characterized by high biological productivity supported by deep upwelling of nutrients and often associated with subsurface Oxygen Minimum Zones (OMZ's). The supply of oxygen to the OMZ is largely controlled by physical, i.e. diffusive and advective, mechanisms, whereas biological processes, i.e. respiration of organic matter, provide sinks (Lachkar and Gruber, 2011).

OMZ's are significant source regions for major climate relevant gases such as carbon dioxide, methane, hydrogen sulfide and nitrous oxide (Paulmier et al., 2008; Paulmier et al., 2011). Processes affecting gas exchange in these regions need to be understood in order to accurately estimate trace gas fluxes from the ocean to the atmosphere and consequences on climate. In 2008, the VAMOS Ocean-Cloud-Atmosphere-Land Study Regional Experiment (VOCALS-REx) and the Chilean Upwelling Experiment (VOCALS-CUpEx) conducted between Southern Peru and Northern Chile focused on the link between aerosols, clouds and precipitation as well as on physical and chemical couplings between the upper ocean and the lower atmosphere (Garreaud et al., 2011; Wood et al., 2011). During the SOPRAN cruise METEOR91 (M91), we studied organic matter components at the very sea surface since properties of the SML may represent a major uncertainty for gas, heat and aerosol fluxes in this specific region and in other oceanic environments. During our cruise, organic matter concentration and composition of the SML and the underlying seawater were studied on 37 different stations, providing the first SML data-set for the upwelling system off Peru, including the first data-set on gel particles in EBU's so far.

2. Material and Methods

2.1. Field information and sampling

The *R*/V METEOR cruise M91 studied the upwelling region off Peru (Bange, 2013). Samples were collected between 4.59° S and 82.0°W, and 15.4°S and 77.5°W from December 03 to 23 in 2012. The overall goal of M91 was to conduct an integrated biogeochemical study on the upwelling region off Peru in order to assess the importance of OMZ's for the sea-air exchange of various climate-relevant trace gases and for tropospheric chemistry. Salinity and temperature were measured with a CTD at each station. Global and UV radiation and wind speed data were retrieved from the DShip database for the time of sampling based on the sensors installed on board.

On 37 different stations between 5°S and 16°S off the Peruvian coast (Figure 1), a total of 39 SML samples was collected from a rubber boat using a glass plate sampler according to the original approach described by Harvey and Burzell (1972). Different methods have been developed to sample and investigate the SML. These methods do not only differ in terms of application but also with respect to the thickness of the SML sampled as well as to selective removal of certain components. Several studies evaluated these methods against each other. A recent summary can be found in the 'Guide to best practices to study the ocean's surface' (Cunliffe and Wurl, 2014). During this study, we applied the glass plate technique because it allows for sampling of a relatively large volume needed to analyze different organic components while keeping the simultaneous sampling of ULW minimal. Two stations were sampled twice in a time frame of 24 hours (stations 12_1 and 12_3, 16_2 and 16_3). Our glass plate with the dimensions of 500 mm (length) x 250 mm (width) x 5 mm (thickness) was made of borosilicate glass and had an effective sampling surface area of 2000 cm^2 (considering both sides). For each sample, the glass plate was inserted into the water perpendicular to the surface and withdrawn

142 slowly at a rate of approximately 20 cm sec^{-1}. The sample, retained on the glass because of
143 surface tension, was removed with the help of a Teflon wiper. Samples were collected as far
144 upwind of the ship as possible and away from the path taken by the ship to avoid contamination.
145 For each sample the glass plate was dipped and wiped about twenty times. The exact number of
146 dips and the total volume collected were recorded. Samples were collected into acid cleaned
147 (HCl, 10%) and Milli-Q washed glass bottles, and the first milliliters were used to rinse the
148 bottles and then discarded. Prior to each sampling, both glass plate and wiper were washed with
149 HCl (10%) and intensively rinsed with Milli-Q water. At the sampling site, both instruments were
150 copiously rinsed with seawater in order to minimize any possible contamination with alien
151 material while handling or transporting the devices.
152 The apparent thickness (d) of the layer sampled with the glass plate was determined as follows:
153 (1) $$d = V/(A \times n)$$
154 Where *V* is the SML volume collected, i.e. 60-140 mL, *A* is the sampling area of the glass plate
155 (*A* = 2000 cm^2) and *n* is the number of dips (Cunliffe and Wurl, 2014). We will use *d* (µm) as an
156 operational estimate for the thickness of the SML.
157 At the same stations, after sampling the SML, about 500 mL samples were collected from the
158 underlying seawater (ULW) at ~ 20 cm depth by holding an acid cleaned (HCl 10%) and Milli-Q
159 rinsed borosilicate glass bottle. The bottle was open and closed underwater to avoid simultaneous
160 sampling of SML water. For safety reasons sampling for the SML from a rubber boat could be
161 made only during daylight hours.
162

163 **2.2 Chemical and biological analyses**

164 **2.2.1. Total organic carbon (TOC) and dissolved organic carbon (DOC)**

Samples for TOC and DOC (20 ml) were collected in combusted glass ampoules, DOC after filtration through combusted GF/F filters (8 hours, 500º C). Samples were acidified with 80 µL of 85% phosphoric acid, heat sealed immediately, and stored at 4°C in the dark until analysis. DOC and TOC samples were analyzed by applying the high-temperature catalytic oxidation method (TOC -VCSH, Shimadzu) modified from Sugimura and Suzuki (1988). The instrument was calibrated every 8-10 days by measuring standard solutions of 0, 500, 1000, 1500, 2500 and 5000 µg C L^{-1}, prepared from a potassium hydrogen phthalate standard (Merck 109017). Every measurement day, ultrapure (MilliQ) water was used to determine the instrument blank, which was accepted for values <1 µmol C L^{-1}. TOC analysis was validated on every measurement day with deep seawater reference (DSR) material provided by the Consensus Reference Materials Project of RSMAS (University of Miami) yielding values within the certified range of 42-45 µmol C L^{-1}. Additionally, two internal standards with DOC within the range of those in samples were prepared each measurement day using a potassium hydrogen phthalate (Merck 109017). DOC and TOC concentration was determined in each sample from 5 to 8 injections. The precision was <4% estimated as the standard deviation of replicate measurements divided by the mean. Particulate organic carbon (POC) was determined as the difference between TOC and DOC.

2.2.2. Total nitrogen (TN) and total dissolved nitrogen (TDN)

TN and TDN were determined simultaneously with TOC and DOC, respectively, using the TNM-1 detector on the Shimadzu analyzer. Nitrogen in the samples is combusted and converted to NOx, which chemiluminesces when mixed with ozone and can be detected using a photomultiplier (Dickson et al., 2007). Calibration of the instrument was done every 8-10 days by measuring standard solutions of 0, 100, 250, 500 and 800 µg N L^{-1}, prepared with potassium nitrate Suprapur® (Merck 105065). Particulate nitrogen (PN) was determined as the difference

between TN and TDN. Deep seawater reference (DSR) material provided by the Consensus Reference Materials Project of RSMAS (University of Miami) was used on every measurement day and yielded values within the certified range of 31-33 µmol N L^{-1}. The precision was <2% estimated as the standard deviation of 5-8 measurements divided by the mean.

2.2.3. Total, dissolved and free amino acids

For total hydrolysable amino acids (THAA), 5 mL of sample were filled into pre-combusted glass vials (8 hours, 500°C) and stored at –20 °C until analysis. Samples for dissolved hydrolysable (DHAA) and free amino acids (FAA) were additionally filtered through 0.45 µm Millipore Acrodisc® syringe filters and then stored in the same way as samples for THAA. Analysis was performed according to Lindroth & Mopper (1979) and Dittmar et al. (2009) with some modifications. Duplicate samples were hydrolyzed for 20h at 100°C with hydrochloric acid (suprapur, Merck) and neutralized by acid evaporation under vacuum in a microwave at 60°C. Samples were washed with water to remove remaining acid. Analysis was performed on a 1260 HPLC system (Agilent). Thirteen different amino acids were separated with a C18 column (Phenomenex Kinetex, 2.6 µm, 150 x 4.6 mm) after in-line derivatization with o-phtaldialdehyde and mercaptoethanol. The following standard amino acids were used: aspartic acid (AsX), glutamic acid (GlX), serine (Ser), arginine (Arg), glycine (Gly), threonine (Thr), alanine (Ala), tyrosine (Tyr), valine (Val), phenylalanine (Phe), isoleucine (Ileu), leucine (Leu), γ- amino butyric acid (GABA). α- amino butyric acid was used as an internal standard to account for losses during handling. Solvent A was 5% acetonitrile (LiChrosolv, Merck, HPLC gradient grade) in sodium-di-hydrogen-phosphate (Merck, suprapur) Buffer (PH 7.0). Solvent B was acetonitrile. A gradient was run from 100% solvent A to 78% solvent A in 50 minutes. FAA were determined from DHAA samples without prior hydrolysis in separate analyses. Particulate

hydrolysable amino acids (PHAA) were determined by subtracting DHAA from THAA. The detection limit for individual amino acids was 2 nmol monomer L^{-1}. The precision was <5%, estimated as the standard deviation of replicate measurements divided by the mean.

2.2.4. Total and dissolved combined carbohydrates

For total and dissolved combined carbohydrates > 1 kDa (TCCHO and DCCHO), 20 mL were filled into pre-combusted glass vials (8 hours, 500 °C) and kept frozen at -20 °C until analysis. Samples for DCCHO were additionally filtered through 0.45 µm Pall Acrodisc® syringe filters. The analysis was conducted according to Engel and Händel (2011) applying high performance anion exchange chromatography coupled with pulsed amperometric detection (HPAEC-PAD) on a Dionex ICS 3000. Samples were desalinated by membrane dialysis (1 kDa MWCO, Spectra Por) for 5 h at 1 °C, hydrolyzed for 20 h at 100°C with 0.4 M HCl final concentration, and neutralized through acid evaporation under vacuum and nitrogen atmosphere (1h, 60 °C) Two replicate samples were analyzed. The retention of carbohydrates on exchange columns, and thus the reproducibility of results are highly sensitive to changes in temperature (Panagiotopoulos et al., 2001; Yu and Mou, 2006). For our system, best resolution of sugars was obtained at 25 °C and therefore applied constantly during all analyses. In order to minimize degradation of samples before analysis, the temperature in the auto-sampler was kept at 4 °C. The system was calibrated with a mixed sugar standard solution including a) the neutral sugars: fucose (4.6 µM, Fuc), rhamnose (3.1 µM, Rha), arabinose (2.0 µM, Ara), galactose (2.4 µM, Gal), xylose/ mannose (3.1 µM, Xyl/ Man), glucose (2.4 µM, Glc), b) the amino sugars: galactosamine (2.0 µM, GalN), glucosamine (2.8 µM, GlcN), and c) the acidic sugars: galacturonic acid (2.8 µM, Gal-URA), gluconic acid (5.1 µM, Glu-Ac), glucuronic acid (3.0 µM, Glc-URA) and muramic acid (1.9 µM, Mur-Ac). Regular calibration was performed by injecting 12.5 µl, 15.0 µl, 17.5 µl and 20 µl of

mixed standard solution. Linearity of the calibration curves of individual sugar standards was verified in the concentration range 10 nM-10 µM. Therefore, the standard mixture was diluted 10, 20, 50, and 100 fold with Milli-Q water. Injection volume for samples and for the blank was 17.5 µl. To check the performance of carbohydrate analysis and stability of the HPLC-PAD system, a 17.5 µl standard solution was analyzed after every second sample. The detection limit was 10 nM for each sugar with a standard deviation between replicate runs of <2%. Milli-Q water was used as blank to account for potential contamination during sample handling. Blanks were treated and analyzed in the same way as the samples. Blank concentration was subtracted from sample concentration if above the detection limit. Particulate combined carbohydrates (PCCHO) were determined as the difference between TCCHO and DCCHO.

2.2.5. Gel particles

Total area, particle numbers and equivalent spherical diameter (d_p) of gel particles were determined by microscopy after Engel (2009). Therefore, 20 to 30 mL were filtered onto 0.4 µm Nuclepore membranes (Whatmann) and stained with 1 mL Alcian Blue solution for polysaccharidic gels, i.e. transparent exopolymer particles (TEP), and 1 mL Coomassie Brilliant Blue G (CBBG) working solution for proteinaceous gels, i.e. Coomassie stainable particles (CSP). Filters were mounted onto Cytoclear© slides and stored at -20 °C until microscopy analysis. The size-frequency distribution of gel particles was described by:

$$\frac{dN}{d(d_p)} = k d_p^{\delta} \quad (2)$$

where dN is the number of particles per unit water volume in the size range d_p to (d_p + $d(d_p)$) (Mari and Kiørboe, 1996). The factor k is a constant that depends on the total number of particles

per volume, and δ (δ < 0) describes the spectral slope of the size distribution. The value δ is related to the slope of the cumulative size distribution $N = a d_p^{\beta}$ by $\delta = \beta + 1$, where N is the total number of particles per unit water volume. The less negative is δ, the greater is the fraction of larger gels. Both δ and k were derived from regressions of $\log(dN/d(d_p))$ versus $\log(d_p)$ over the size range 1.05-14.14 µm ESD.

Formation of exopolymeric gel particles, e.g. TEP, can be described in terms of coagulation kinetics (Engel et al., 2004; Mari and Burd, 1998). Aggregates can be described using a fractal scaling relationship, e.g. $M \sim L^D$, where M is the mass of the aggregate, L the size and D is the fractal dimension, which is controlled by the size of particles that form the aggregate as well as by the processes of particle collision, e.g Bownian Motion, shear, or differential settlement (Meakin, 1991). Assuming that TEP are formed by shear induced coagulation D can be estimated from δ (Mari and Burd, 1998):

(3) $$D = \frac{(64 - \partial)}{26.2}$$

2.2.6. Heterotrophic bacteria

For bacterial cell numbers, 4 mL samples were fixed with 200 µL glutaraldehyde (25% final concentration) and stored at –20°C until enumeration. Samples were stained with SYBR Green I (Molecular Probes). Heterotrophic bacteria were enumerated using a flow cytometer (Becton & Dickinson FACScalibur) equipped with a laser emitting at 488 nm and detected by their signature in a plot of side scatter (SSC) versus green fluorescence (FL1). Heterotrophic bacteria were distinguished from photosynthetic prokaryotes (e.g. *Prochlorococcus*) by their signature in a plot of red fluorescence (FL2) versus green fluorescence (FL 1). Yellow-green latex beads

(Polysciences, 0.5 µm) were used as internal standard. Sampling bacterioneuston with a glass plate does not bias cell abundance measurements (Stolle et al., 2009).

2.2.7. Phytoplankton

For photoautotrophic cell numbers <20 µm, 4 mL samples were fixed with 20 µL glutaraldehyde (25% final concentration), and stored at –80°C until enumeration. Phytoplankton counts were performed with a FACSCalibur flow-cytometer (Becton Dickinson) equipped with an air-cooled laser providing 15 mW at 488 nm and with a standard filter set-up. The cells were analyzed at high flow rate (~39-41 µL min^{-1}) with the addition of 1µm-fluorescent beads (Trucount, BD). Autotrophic groups were discriminated on the basis of their forward or right angle light scatter (FALS, RALS) as well as from chlorophyll and phycoerythrin (characteristic for cyanobacterial, mainly *Synechococcus* populations) fluorescence. Cell counts were analyzed using BD CellQuest Pro-Software. Two groups were distinguished: Non-cyanobacterial-type phytoplankton (NCPL) and cyanobacterial-type phytoplankton (CPL).

2.3. Data analysis

The relative concentration of a substance A in the SML was compared to the underlying water (ULW) by the enrichment factor (EF), defined by:

$$EF = (A)_{SML} / (A)_{ULW} \quad (4)$$

Where (A) is the concentration of a given parameter in the SML or ULW, respectively (GESAMP, 1995). Because the concentration of a component is normalized to its values in the underlying water, EF for different components can be readily compared. Enrichment of a component is indicated by EF > 1, depletion by EF < 1.

Differences in data as revealed by statistical tests (*t*-test) were accepted as significant for $p < 0.05$. Average values for total concentrations are given by their arithmetic mean, averages for ratios by their geometric mean. Average values are reported with ±1 standard deviation (SD). Calculations, statistical tests and illustration of the data were performed with the software packages Microsoft Office Excel 2010, Sigma Plot 12.0 (Systat) and Ocean Data View (Schlitzer, 2013). Weighted-average gridding was used in ODV to display data in the SML according to data coverage with automatic scale lengths (53 permille x-scale length, 40 permille y-scale length).

3. Results

3.1. The physical environment

Coastal upwelling off Peru can occur throughout the year (Carr and Kearns, 2003). During the M91 cruise upwelling and upwelling velocities were determined from $^{3}He/^{4}He$ disequilibrium (Steinfeldt et al., 2015). High upwelling velocities of $>3x10^{-5}$ m s^{-1} were observed south of Lima (stations 10, 14, 15) (Figure 1). The coastal upwelling of deep water resulted in strong gradients of surface seawater temperature and salinity along the Peruvian shelf as well as with increasing distance to the shelf during M91. Salinity measured at about 1 m depth corresponding to the ship's keel varied between 32 and 35 with the lowest values occurring close to the coast at stations 10_1 to 10_4, 14_1 and 14_2 and 15_1 to 15_3 Here, temperatures were below the average of all surface stations (19.25±1.7°C), indicating the colder, upwelling deep water (Table 1, Figure 2). Wind speed encountered during the cruise ranged between 0.6 and 9.0 m s^{-1} with the lower wind speeds also observed closer to the coast, i.e. between 12° and 14°S and at the northern stations (Figure 2). Thus, higher wind speed was observed at the more off-shore stations having higher surface water temperatures, leading to significant co-variation between surface water temperature and wind speed (Figure 3). Global radiation and UV radiation varied between

10 and 1103 W m^{-2}, and between 0.8 and 71 W m^{-2}, respectively, with no significant impact of SML organic matter accumulation.

3.2. SML properties and organic matter accumulation

Estimates for SML thickness are depending on the method applied to sample the SML (Carlson, 1982; Zhang et al., 1998). For the glass plate technique, Zhang et al. (1998) showed that SML thickness decreases with increasing withdrawal rates; i.e. from 50-60 µm for a withdrawal rate of 20 cm s^{-1}, to 10-20 µm at rate of 5-6 cm s^{-1}. Their results confirmed earlier studies that generally revealed thinner SML layers at slower withdrawal rates (Carlson, 1982; Harvey and Burzell, 1972; Hatcher and Parker, 1974). During this study, the SML was sampled with the glass plate at ~20 cm s^{-1}, yielding a thickness between 45 and 60 µm, with an overall mean value of 49± 8.89 µm (n=39). This value is in good accordance with the proposed apparent sampling thickness of 50±10 µm (Zhang et al., 1998) and fits well to previous observations for the SML sampled with a glass plate at the same withdrawal rate (Cunliffe et al., 2011; Galgani and Engel, 2013; Galgani et al., 2014; Zhang et al., 1998; Zhang, 2003). Using direct pH microelectrode measurements, Zhang (2003) later confirmed an *in situ* thickness of ~60 µm for the SML, which they defined as the layer of sudden change of physico-chemical properties.

We therefore assume that samples obtained from the SML during this study well represented the SML, as defined by Zhang (2003). Thickness of the SML as determined during this study increased significantly with amount of organic substances in the SML, determined as TOC concentration (p<0.005; n=39). This corroborates earlier findings from experimental studies showing that organic matter produced by phytoplankton increases the thickness of SML sampled with a glass plate (Galgani and Engel, 2013). No correlation instead was observed between SML

thickness and wind speed (r=-0.11, n=39) or between SML thickness and temperature (r=-0.06; n=39).

Unless stated otherwise, all observations described in this paragraph relate to the SML. In general, concentration of organic components in the SML showed spatial distribution patterns resembling those of temperature and wind speed (Figures 3, 4, 5). Highest concentration values for nearly all organic components were observed at the upwelling stations 10_1 to 10_4, 14_1 and 14_2 and 15_1 to 15_3 (Figure 1) in accordance with high estimated primary production rates (Steinfeldt et al., 2015) and high Chl *a* concentrations (Hu et al., 2015) determined in surface waters at these sites during M91.

Phytoneuston abundances (<20 µm) varied between $3.7x10^3$ and $1.9x10^5$ mL^{-1} for cyanobacterial-type phytoplankton (CPL) (mainly *Synechococcus spp.*) and between $5.4x10^3$ and $3.0x10^5$ mL^{-1} for other non-cyanobacterial-type phytoplankton (NCPL). Generally, highest abundance was determined on and close to the upwelling stations (Figure 4). On all other stations, cell abundance of CPL and NCPL differed spatially, with higher abundance of NCPL at the southern stations and higher numbers of CPL at the northern stations (Figure 4). NCPL and CPL were closely related to cell abundance in the ULW (Table 3).

Heterotrophic bacteria were determined in abundances between $3.0x10^4$ and $8.5x10^6$ mL^{-1} with highest numbers observed at the upwelling stations and southeast of the upwelling (Figure 4). Heterotrophic bacteria in the SML were highly positively correlated to abundances in the ULW (r=0.94; n=36; p<0.001) and negatively influenced by wind speed, although less clearly (r=-0.37; n=36; p=0.01). No significant influence on heterotrophic bacteria abundance was detected with respect to global radiation or UV radiation.

TOC concentration ranged between 82 and 199 µmol L^{-1}, and was clearly higher than DOC concentration on all stations. Particulate Organic Carbon (POC) concentration was calculated as the difference between TOC and DOC and ranged from 2.3 to 96 µmol L^{-1}. Highest POC concentration was observed at the upwelling stations (Figure 5). In general, POC concentration was highly correlated to temperature (r=-0.67, n=39 p<0.001) and to wind speed (r= -0.48, n=39 p<0.001) (Table 3). DOC concentration ranged between 71 and 122 µmol L^{-1} (Table 2) and, in contrast to POC, was not significantly related to temperature or wind speed (Table 3). Relatively high DOC concentrations of about 100 µmol L^{-1} were observed at stations 9 and 9_2 (Figure 5), but excluding these stations from analysis did not reveal a correlation to temperature or wind speed either. DOC is a bulk measure and is quantitatively dominated by refractory compounds that are independent from recent biological productivity. More closely linked to productivity and likely stimulated by the upwelling of nutrients along the Peruvian coast are labile and semi-labile compounds such as dissolved combined carbohydrates and amino acids. Indeed, both DCCHO and DHAA reached highest concentrations at the upwelling stations (Figure 5). Thereby, maximum concentration of DCCHO of 2670 nmol L^{-1} (mean: 1110±550 nmol L^{-1}) was observed at station 15_2, slightly south of the station 14_1 exhibiting highest DHAA concentrations of 2020 nmol L^{-1} (mean: 770 ± 360 nmol L^{-1}) (Table 2). In general high DCCHO concentration was more focused to the upwelling, and exhibited strong horizontal gradients to the northern and southern stations.

DHAA concentration was on average lower than DCCHO concentration (Table 2) and horizontal differences were less pronounced than for DCCHO. Both components of semi-labile DOC were inversely correlated to temperature (DCCHO r=-0.44, n=39, p<0.001; DHAA: r=-0.47, n=30, p<0.001), linking their accumulation in the SML to productivity in the cold upwelling waters.

Concentrations of carbohydrates and amino acid in particles, and in gels (i.e. TEP, CSP) in particular, were highest at the coastal upwelling stations also. Particulate carbohydrates and amino acids (PCCHO, PHAA) were highly correlated to POC concentrations (PCCHO: r=0.70, n=39, p<0.001; PHAA: r=0.81, n=30, p<0.001).

In general, numerical abundance as well as total area were about 10-fold higher for CSP than for TEP (Table 2). Spatial variability of gel particles abundance was high, and yielded lowest values of total TEP area of 6.9 mm^2 L^{-1} at station 13_1 and highest values of 408 mm^2 L^{-1} at station 15_1, about 100 nautical miles apart. The highest abundance of both TEP and CSP was observed close to the coastal upwelling, but apart from these stations, the distribution of TEP in the SML clearly differed from that of CSP (Figure 5). While higher TEP abundance was observed at the northern stations, CSP abundance was more pronounced at the southern stations. Moreover, stations of highest and lowest concentration of CSP were different from those of TEP. Lowest value of CSP total area of 137 mm^2 L^{-1} was observed at station 11_1 and highest values of 3051 mm^2 L^{-1} at station 14_1.

3.3. Accumulation patterns in the SML

For almost all components investigated during this study, concentration in the SML was significantly related to the respective concentration in the ULW (Table 3). Thereby, correlations between SML and ULW were strongest for combined carbohydrates, particularly for DCCHO. Close correlations were also observed for bulk organic carbon measurements, i.e. TOC, DOC, and derived therefrom POC. For dissolved nitrogenous compounds, i.e. TDN, FAA and DHAA no relationship between SML and ULW concentrations was observed, suggesting that loss or gain of these compounds in the SML were faster than exchange processes with the ULW. Temperature had an effect on most organic compounds in the SML, with generally higher

concentrations at lower temperature (Table 3). This can largely be attributed to the higher production of organic matter at the colder upwelling sites. Concentrations of particulate components POC, TEP, PHCHO, PHAA and particulate nitrogen (PN) were also inversely related to wind speed, whereas DCCHO and DHAA were inversely related to temperature but not to wind speed. Clear differences were observed for the two different gel particle types determined in this study. In contrast to TEP, neither abundance nor total area of CSP were related to wind speed, nor to seawater temperature. Instead abundance of CSP in the SML was mostly related to their abundance in ULW. However, with the exception of CSP, particulate components in the SML were affected by changes in wind speed more than concentration of dissolved compounds (Table 3).

Enrichment factors indicated a general accumulation of organic matter in the SML with respect to the ULW (Figure 6), which happened at most stations. Thereby, clear differences were observed between EF values of different components. The highest enrichment was observed for FAA that were enriched more than 10-fold at some stations. Moreover, FAA were consistently enriched in the SML, except for one station where the lowest FAA concentration was determined (49 nmol L^{-1}). The largest variability of EF was observed for abundance and total area of gel particles. For TEP total area, values of EF ranged between 0.2-12, with highest EF observed at the coastal upwelling station 14_1, where the wind speed recorded was 0.6 m s^{-1}. In proximity of this station, the lowest EF of TEP was determined (station 15_3) indicating a clear depletion at wind speed of 7 m s^{-1}. The EF of CSP total area ranged between 0.4 and 4.8. Thus highest EF of CSP was clearly lower than for TEP, and in contrast to TEP it was observed at the more offshore station 18_2 at a higher wind speed rate of 9.2 m s^{-1}. Total and dissolved hydrolysable amino acids (THAA, DHAA) were enriched in the SML at almost all stations (Figure 6), with EF in the range

452 0.8 - 4.6 (DHAA) and 0.4 - 3.4 (THAA). Median EFs were 1.7 and 1.4 for DHAA and THAA,
453 respectively.
454 Concentration of TCCHO and DCCHO in the SML were often similar to the ULW, with EF
455 values ranging between 0.6 and 1.4 (DCCHO) and between 0.3 and 1.7 (TCCHO), respectively.
456 In general, variability of EF was smaller for dissolved than for particulate organic compounds,
457 suggesting differences in the accumulation dynamics.
458 In contrast to all organic, chemical compounds, bacteria were found to be depleted in the SML at
459 almost all stations (Figure 6), having a median EF of 0.8
460

461 **3.4. Size distribution of gel particles within the SML**

462 Abundance of gel particles in the SML and ULW decreased with increasing particle size
463 according to the power law function given in eq. 2 (Figure 8). The parameter δ describes the
464 slope of the particles size spectrum. Lower values of δ indicate relatively higher abundance of
465 smaller particles. Data fits to the function were very well described for each sample with r^2>0.90,
466 yielding a standard error for δ of <20%. For TEP, δ varied between -2.63 and -1.38 (mean
467 value: -1.86, SD: 0.27) for particles in the SML and between -2.25 and -1.25 (mean value: -1.70,
468 SD: 0.30) for particles in the ULW. To compare the size distribution of TEP in the SML and the
469 ULW, we calculated the slope ratio ($\delta^* = \delta_{SML} / \delta_{ULW}$) (Figure 9). Size distributions of TEP in the
470 SML and ULW were generally quite similar yielding δ^*_{TEP} in the range of 0.78-1.42, with a
471 median value of 1.1. Nevertheless, spatial differences were observed, with δ^*_{TEP} <0.95 at the
472 more coastal northern stations and δ^*_{TEP} >1.1 more offshore at the southern stations (Figure 9). At
473 the upwelling stations with high TEP abundance slopes of SML and ULW were very similar,
474 yielding δ^*_{TEP} in the range 0.95 - 1.1. This showed a relatively higher abundance of smaller TEP
475 in the SML at the offshore stations, whereas relatively more, larger sized TEP were present close

476 to the coast in the northern part of the study region. This comparison also showed that sampling
477 of TEP from the SML with a glass plate does not bias TEP size distribution, e.g. by inducing
478 particle aggregation during sampling. Such a bias would be expected especially at stations where
479 TEP was highly abundant, like at the upwelling stations. However, particularly at those stations
480 no differences in size distributions of TEP in the SML and ULW were observed. Fractal scaling
481 exponents of TEP were estimated from eq. 3 and yielded D=2.51 for both SML and ULW
482 samples (D_{SML}=2.51±0.015; D_{ULW}=2.51±0.011). The very similar fractal dimension for TEP in
483 the SML and ULW suggests that TEP in the SML and in the bulk water are formed by similar
484 aggregation processes. The value of D=2.51 estimated in this study is close to 2.55 proposed by
485 Mari and Burd (1998) for seawater TEP.
486 In the SML, the number of TEP in the smallest size class (1.25-1.77 µm) ranged from 96 to
487 1.38×10^4 mL^{-1}, and included on average 61±5.2% of all TEP. For CSP, variability of abundance
488 in the 1.25-1.77 µm size class was much smaller and ranged between 1.46×10^4 and 2.33×10^5 mL^{-1}.
489 Although CSP thus represented the largest fraction of small gel particles, the relative
490 abundance of CSP in the smallest size fraction was lower, yielding an average contribution of
491 52±6.0% of all CSP. Similar to TEP, size distribution of CSP followed the power law
492 relationship of eq. 2, yielding δ values between -1.12 and -2.01 (mean value: -1.44, SD: 0.20) for
493 particles in the SML and between -1.11 and -1.88 (mean value: -1.39, SD: 0.17) for particles in
494 the ULW. With D=2.50±0.008, the fractal dimension of CSP was almost identical to that of TEP,
495 suggesting that similar processes, i.e. shear induced aggregation, are responsible for CSP
496 formation. The slope ratio, δ^*, for CSP varied between 0.77 and 1.32, with a median value of 1.0.
497 No spatial pattern was observed for the distribution of δ^*_{CSP}. Slopes of the size distribution of
498 CSP in the SML and ULW were not significantly different (p=0.176, n=39, paired t-test),

499 indicating that CSP size distribution, similarly to TEP, is not biased by the sampling approach of
500 the glass plate.
501 No overall relationship was established between the slope of the size distribution of TEP and
502 wind velocity (δ_{TEP} vs. wind speed: r=-0.19, n= 37, p=0.20). However, TEP size distribution was
503 much steeper at the station with highest wind speed compared to the one with lowest wind
504 velocity (δ_{TEP} at 0.6 m s^{-1}= -1.51, r^2=0.95, n=7; δ_{TEP} at 9.0 m s^{-1}= -2.31, r^2=0.95, n=7) (Figure
505 8a). In particular, at the high wind speed a loss of larger TEP, i.e. >7 µm was observed in the
506 SML compared to the ULW and relative to the low wind speed station.
507 For CSP a significant inverse relationship was observed between the slope δ and wind speed
508 (δ_{CSP} vs. wind speed: r=-0.61, n=37, p<0.001). A loss of larger CSP was also observed by direct
509 comparison between low and high wind speed stations (δ_{CSP} at 0.6 m s^{-1}= -1.12, r^2=0.92, n=7;
510 δ_{TEP} at 9.0 m s^{-1}= -1.45, r^2=0.97, n=7) (Figure 8b).
511

512 **4. Discussion**

513 It has been suggested that the presence of organic matter in the SML influences a series of
514 processes relevant to air-sea exchange of gases, dissolved and particulate components. EBU'S are
515 characterized by high biological productivity and strong across shelf gradients of organic matter
516 concentration (Capone and Hutchins, 2013). Therefore EBU'S are ideal model systems to study
517 the linkages of biological productivity and SML properties, with respect to characteristics of
518 organic matter composition and factors controlling organic matter enrichment in the SML.
519

520 **4.1. Organic matter characteristics of the SML in the upwelling region off Peru**

521 Strong horizontal gradients in organic matter concentration of the SML were observed for the
522 coastal and shelf-break region off Peru with generally higher organic matter concentrations in the

SML towards the area of upwelling of colder, nutrient-rich deep water. Hence, increasing ecosystem productivity is one likely factor responsible for higher concentrations of organic components in the SML. Significant correlations between organic matter concentration in the SML and in the ULW were determined and showed that the SML basically reflects the underlying seawater system. The close connectivity between SML organic properties and biological development was also shown during a recent mesocosm study, indicating that ecosystem changes impact SML organic matter composition and concentration (Galgani et al., 2014). Despite this finding that relates to a more general characteristic of the SML, clear differences in the accumulation behavior of different organic matter components were determined during this study and are in good accordance with previous observations. A generally higher SML accumulation was observed for amino acids compared to carbohydrates. Significant enrichment of amino acids in the SML has been determined previously for coastal as well as open ocean sites, and higher accumulation of FAA compared to DHAA and THAA, as also observed during this study, appears to be a consistent SML feature (Carlucci et al., 1992; Henrichs and Williams, 1985; Kuznetsova and Lee, 2002, 2001; Kuznetsova et al., 2004; Reinthaler et al., 2008). As for this study, wind velocity and temperature have not been identified as physical factors responsible for amino acid enrichment in the past (Kuznetsova et al., 2004). FAA and DHAA are labile to semi-labile substrates and taken-up by heterotrophic microorganisms (Keil and Kirchman, 1992). Turnover times of these components in the water column are usually in the range of minutes to days (Benner, 2002; Fuhrman and Ferguson, 1986). The observed accumulation of FAA and DHAA in the SML may therefore be related to a reduced activity of bacteria. For different coastal Baltic Sea sites, Stolle et al. (2009) determined a lowered bacterial biomass production in the SML, despite bacterial cell numbers being similar to those in the ULW. During M91 bacteria were mostly depleted in the SML compared to the ULW supporting

547 the idea of the SML being an ‘extreme environment’ for bacteria. Earlier studies showed that
548 some bacteria may be adapted to UV radiation in the SML as well as in the ULW (Agogué et al.,
549 2005; Carlucci et al., 1985). Amino acid consumption by bacterioneuston under UV-B stress may
550 be reduced (Santos et al., 2012), which may give an explanation for the higher concentrations of
551 FAA and DHAA in the SML during M91. However, no significant correlation between bacterial
552 abundance and UV radiation or between UV radiation and amino acid concentrations in the
553 different pools was observed during this study, suggesting that at most stations history rather than
554 instantaneous UV radiation is if at all responsible for controlling bacteria and organic matter
555 components in the SML.
556 SML thickness during this study was significantly related to TOC concentration, but not to wind
557 speed. A thickening of the SML with increasing wind speed up to 8 m s^{-1} has been observed by
558 Falkowska (1999) from samples collected in the Baltic Sea and explained by increased advective
559 transport of organic matter to the SML, e.g. through bubble adsorption, at higher turbulence.
560 During M91, accumulation of organic matter in the SML was higher at the upwelling stations
561 where wind speed often was quite low. Hence, a higher source of organic matter in the ULW may
562 have counterbalanced the wind speed effect.
563
564 Wind speed, however, was determined as a factor controlling accumulation of particulate
565 material, in particular TEP, in the SML in addition to the dynamics occurring in the ULW. TEP
566 are marine gel particles hypothesized to be neutrally or positively buoyant thanks to their high
567 water content (Azetsu-Scott and Passow, 2004; Engel and Schartau, 1999). TEP were moreover
568 suggested to form within the SML, either by wind-shear induced aggregation of precursors or due
569 to coalescence of pre-cursor molecules, primarily polysaccharides, when entrained air bubbles
570 burst at the sear surface (Wurl et al., 2011). Adsorption of DOM onto bubble surfaces and TEP

formation by bubble bursting have been determined during experimental flotation and bubbling studies using surface seawater from different locations (Wallace and Duce, 1978; Zhou et al., 1998). Bubble scavenging of DOM in the upper water column may thus be responsible for high concentrations of TEP at the SML, because more TEP precursors are lifted up the water-column (Gao et al., 2012; Wurl et al., 2011). In addition, compression and dilatation of the SML due to capillary waves may increase the rate of polymer collision, subsequently facilitating gel aggregation (Carlson, 1993). During M91, TEP enrichment in the SML was inversely related to wind speed, supporting earlier observations of Wurl and colleagues (Wurl et al., 2009; Wurl et al., 2011). However, in contrast to earlier observations showing EF values >1 for TEP in the SML also at higher wind speed, we found the SML to be depleted of TEP at wind speed of ~ 5 m s^{-1} and above. It has been suggested that TEP aggregation rates in the SML are higher than in the ULW, due to enhance collision rates by shear or bubble bursting. TEP have been shown to control coagulation efficiencies of solid particles, such as diatoms and coccolithophores (Chow et al., 2015; Engel, 2000; Logan et al., 1995). At higher wind speed, increased aggregation rates of TEP with solid particles, eventually containing mineral ballast, may thus favor the formation of aggregates that become negatively buoyant and sink out of the SML. This, may explain the observed loss of larger TEP (>7 µm) from the SML relative to the ULW and to the SML at low wind speed. Enhanced aggregation rates could then also explain the inverse relationship between POC and wind speed, observed during this study.

In contrast to TEP, no impact of wind speed was determined for CSP accumulation, or for CSP enrichment in the SML. Moreover, clear spatial differences were observed for the distribution of TEP and CSP in the SML. Although both TEP and CSP are gel particles that form from dissolved organic precursors released by microorganisms, their spatial and temporal occurrence in marine

595 systems can be quite different, e.g. TEP accumulate towards the end of phytoplankton blooms
596 while CSP rather co-occur with maximum phytoplankton abundance (Cisternas-Novoa et al.,
597 2015; Engel et al., 2015). Moreover, the depth distribution of TEP and CSP was shown to be
598 different for open ocean sites (Cisternas-Novoa et al., 2015). These spatial and temporal
599 differences in the occurrence of TEP and CSP in the water column may explain the spatial
600 separation of both types of marine gels in the SML observed during this study. However, the
601 observed differences in relation to wind speed suggest that additional factors control the
602 enrichment of TEP and CSP in the SML. It has been shown that CSP are less prone to
603 aggregation than TEP (Engel et al., 2015; Prieto et al., 2002). Similarly, CSP may be less
604 involved in aggregation formation and sinking out of the SML at higher wind speed. Yet,
605 similarly to TEP, larger CSP were observed in the SML at low wind speed suggesting that both
606 kind of gels may be involved in slick formation that becomes disrupted when wind speed
607 increases.
608
609
610 **4.2. Implications of organic matter accumulation in EBUS**
611 **4.2.1. Air-Sea gas exchange**
612 Although the SML and surface active substances (surfactants) within are widely believed
613 affecting the exchange of gases and heat at the air-sea interface (Davies, 1966; Frew, 1997; Salter
614 et al., 2011), particularly at lower wind speed (Liss, 1983), we still have little quantitative
615 knowledge on how natural organic components at the immediate sea-surface alter the gas transfer
616 velocity in water (*kw*). Our data showed a depletion of the SML with respect to TEP and POC at
617 wind speeds >5 m s^{-1}, suggesting that an effect of these 'insoluble' components on gas exchange
618 is, if any, operating only at low wind speed. Due to their fractal scaling, gel particles have a

relatively large surface to volume ratio and may act as a cover, reducing molecular diffusion rates at the interface between air and sea.

Accumulation of dissolved organic components in the SML during M91 was not related to wind speed. DCCHO and DHAA concentration representing fresh DOM were highest at the upwelling sites and therefore negatively related to seawater temperature. DOM, such as DCCHO and chromophoric dissolved organic matter (CDOM), have demonstrated surfactant properties and reduced gas transfer velocity in water (*kw*) at low wind speed in laboratory and field experiments (Frew et al., 2004; Frew et al., 1990). The reduction of *kw* is thereby believed to be related to a dampening of small, capillary waves. Salter et al. (2011) recently showed that artificial surfactants can suppress gas transfer velocity by up to 55% at sea. Suppression of k666 (i.e. *kw* normalized to a Schmidt number of 666) during their field study was depending on wind speed, but was detected up to 11 m s^{-1}, encompassing the full range of wind speed determined during M91. Thus, accumulation of natural DOM particularly in upwelling regimes with high biological production and coastal wind shelter as observed during this study may have an influence on gas exchanges rates as well.

Across the SML, the diffusivity of climate relevant gases such as methane (CH_4), has been proposed being mediated by SML bacteria, as possible sink (Upstill-Goddard et al., 2003) or source of this compound (Cunliffe et al., 2013). About ~ 30 % of the atmospheric concentration of nitrous oxide (N_2O), one of the strongest greenhouse gases and responsible for ozone depletion, is supported by oceanic sources (Solomon et al., 2007). Of total oceanic N_2O production, oxygen minimum zones (OMZs) contribute about 25-75 % (Bange et al., 2001). In EBU'S, high primary production and induced high aerobic remineralization associated with large-scale circulation maintain the presence of OMZs (Gutknecht et al., 2013; Paulmier and

643 Ruiz-Pino, 2009), which, in the last decades, have been expanding and intensifying due to
644 enhanced stratification and reduced ventilation (Keeling et al., 2010; Stramma et al., 2008).
645 During M91, N_2O concentration in surface waters was highly supersaturated at the upwelling
646 sites and in particular at station 14_1 (Arevalo-Martinez et al., 2015). Although a direct influence
647 of organic matter in the SML on gas-exchange was not investigated during M91, it can be
648 assumed that the high enrichment of organic components in the SML observed the upwelling
649 sites was one factor contributing to N_2O supersaturation.
650 Our study was intended to understand how organic matter accumulates in the SML, which might
651 mediate the transfer rate of trace- and greenhouse gases such as N_2O in oceanic regions like
652 OMZ's affected by a changing climate. A recent laboratory study reported π non-covalent
653 interactions of N_2O with phenols, suggesting a possible important role of N_2O in biological
654 processes by specifically binding to phenolic groups as those of the amino acids tyrosine and
655 phenylalanine (Cao et al., 2014). Tyrosine and phenylalanine in the SML of our study represented
656 a small molar percentage of total amino acids pool (data not shown), but were present. As we
657 found evidence of overall amino acids SML accumulation during our cruise, for those amino
658 acids in particular the median EF both in the total (THAA) and in the dissolved (DHAA) fraction
659 was > 1, suggesting a possible interaction of specific SML organics with N_2O in the coastal
660 upwelling region off Peru. Although the experiment conducted by Cao and colleagues cannot be
661 directly translated to our setting, it provides interesting ideas for the interaction of N_2O with
662 biological macromolecules worth further investigation.
663 Overall, our results showed that accumulation of organic substances occurs in EBU's and is
664 related to the increased biological production. Hence, the organic SML may play a particularly
665 important role for exchange of climate relevant gases that are associated to high organic matter
666 production and resulting anoxia in upwelling systems like the one off Peru.

667 **4.2.2. Organic aerosol production**

668 The structure of sea-spray aerosols (SSA) originating by bubble bursting at the sea surface is a
669 function of biological, chemical and physical properties of the SML, which may comprise a vast
670 array of organic surface-active compounds, microorganisms, and exopolymer gels (Leck and
671 Bigg, 2005; Quinn and Bates, 2011; Wilson et al., 2015). Despite recent evidences showing that
672 high levels of chlorophyll-*a* are not directly related to the organic carbon content of SSA (Quinn
673 et al., 2014), still organic SSA largely derive from the oceanic surface layer and therefore are also
674 subject to the effects of climate change on marine systems (Andreae and Crutzen, 1997).
675 Polysaccharides and polysaccharidic nanogels (Orellana et al., 2011; Russell et al., 2010) as well
676 as particulate amino acids and proteinaceous compounds (Kuznetsova et al., 2005) are present in
677 organic SSA particles. During M91, we found a different accumulation behavior of TEP and CSP
678 in the SML. TEP showed a close inverse relationship to wind speed, being depleted in the SML
679 above 5 m s^{-1}, while particulate proteinaceous compounds (CSP) accumulated independently of
680 wind speed. Submicron gels embedded in sea spray may represent an important source for
681 primary organic aerosols in the more offshore wind exposed regions. TEP as well as dissolved
682 polysaccharides include sugars with carboxylic groups such as uronic acids and may contribute to
683 the relatively high fraction of carboxylic acid that was observed in the organic matter component
684 of marine aerosols (Hawkins et al., 2010). In the upwelling region off Peru the wind-driven
685 export of polysaccharidic components to the atmosphere thus might represent a loss-pathway of
686 these organic compounds from the SML that would then contribute to a larger extent to the
687 organic SSA mass. Proteinaceous compounds, including CSP, are probably more stable at the sea
688 surface and may contribute to organic mass in aerosols even at higher wind speed.

689 However, future studies that investigate gel particles within the SML and in SSA are needed to
690 clarify if the observed loss of TEP from the SML at higher wind speeds is indeed related to a
691 transport of TEP to the atmosphere, or if CSP contribute to organic aerosol mass.
692 The accumulation of organic matter in the SML, and the distinct behavior of certain compounds
693 at the water-air interface is certainly an important issue for all exchange processes between the
694 ocean and the atmosphere that needs to be further exploited.
695
696
697 **Acknowledgements**
698
699 We thank the captain and crew of *R*/V METEOR during cruise leg M91 for logistic support
700 during sampling, especially help related to the rubber boat operation, as well as H. Bange as chief
701 scientist and all the scientific crew. A great acknowledgement goes to J. Roa for helping with
702 SML sampling on board and for TOC/TN and carbohydrates analysis, respectively. Further
703 technical help was provided by *R*. Flerus, S.Manandhar and N. Bijma for amino acids and
704 microscopy analysis, as well as T. Klüver for flow-cytometry counts. This work was supported
705 by BMBF project SOPRAN II and III (Surface Ocean Processes in the Anthropocene, 03F0611C-
706 TP01 and 03F0662A-TP2.2).
707

References:

Agogué, H., Casamayor, E. O., Bourrain, M., Obernosterer, I., Joux, F., Herndl, G. J., and Lebaron, P.: A survey on bacteria inhabiting the sea surface microlayer of coastal ecosystems, FEMS Microbiology Ecology, 54, 269-280, 2005.

Andreae, M. O. and Crutzen, P. J.: Atmospheric Aerosols: Biogeochemical Sources and Role in Atmospheric Chemistry, Science, 276, 1052-1058, 1997.

Arevalo-Martinez, D. L., Kock, A., Loscher, C. *R*., Schmitz, *R*. A., and Bange, H. W.: Massive nitrous oxide emissions from the tropical South Pacific Ocean, Nature Geosci, 8, 530-533, 2015.

Azetsu-Scott, K. and Passow, U.: Ascending marine particles: significance of transparent exopolymer particles (TEP) in the upper ocean. , Limnol. Oceanogr., 49, 741-748, 2004.

Bange, H. W.: Surface Ocean - Lower Atmosphere Study (SOLAS) in the upwelling region off Peru - Cruise No. M91 – December 01 – December 26, 2012 – Callao (Peru) – Callao (Peru), Bremen, 69 pp., 2013.

Bange, H. W., Rapsomanikis, S., and Andreae, M. O.: Nitrous oxide cycling in the Arabian Sea, J. Geophys. Res-Oceans, 106, 1053-1065, 2001.

Bar-Zeev, E., Berman-Frank, I., Girshevitz, O., and Berman, T.: Revised paradigm of aquatic biofilm formation facilitated by microgel transparent exopolymer particles, Proceedings of the National Academy of Sciences, 109, 9119-9124, 2012.

Benner, *R*.: Chemical composition and reactivity. In: Biogeochemistry of marine dissolved organic matter, Hansell, D. A. and Carlson, D. J. (Eds.), Academic Press - Elsevier, 2002.

Bigg, K. E., Leck, C., and Tranvik, L.: Particulates of the surface microlayer of open water in the central Arctic Ocean in summer, Mar. Chem., 91, 131-141, 2004.

Cao, Q., Gor, G. Y., Krogh-Jespersen, K., and Khriachtchev, L.: Non-covalent interactions of nitrous oxide with aromatic compounds: Spectroscopic and computational evidence for the formation of 1:1 complexes, J. Chem. Phys., 140, 144304, 2014.

Capone, D. G. and Hutchins, D. A.: Microbial biogeochemistry of coastal upwelling regimes in a changing ocean, Nat. Geosci., 6, 711-717, 2013.

Carlson, D.: The Early Diagenesis of Organic Matter: Reaction at the Air-Sea Interface. In: Organic Geochemistry, Engel, M. and Macko, S. (Eds.), Topics in Geobiology, Springer US, 1993.

Carlson, D. J.: A field evaluation of plate and screen microlayer sampling techniques, Mar. Chem., 11, 189-208, 1982.

Carlucci, A. F., Craven, D. B., and Henrichs, S. M.: Surface-film microheterotrophs: amino acid metabolism and solar radiation effects on their activities, Marine Biology, 85, 13-22, 1985.

Carlucci, A. F., Wolgast, D. M., and Craven, D. B.: Microbial Populations in Surface Films: Amino Acid Dynamics in Nearshore and Offshore Waters off Southern California, J. geophys. Res., 97, 5271-5280, 1992.

Carr, M.-E. and Kearns, E. J.: Production regimes in four Eastern Boundary Current systems, Deep Sea Research Part II: Topical Studies in Oceanography, 50, 3199-3221, 2003.

Chin, W.-C., Orellana, M. V., and Verdugo, P.: Spontaneous assembly of marine dissolved organic matter into polymer gels, Nature, 391, 568-572, 1998.

Chow, J. S., Lee, C., and Engel, A.: The influence of extracellular polysaccharides, growth rate, and free coccoliths on the coagulation efficiency of Emiliania huxleyi, Marine Chemistry, doi: http://dx.doi.org/10.1016/j.marchem.2015.04.010, 2015. 2015.

752 Cisternas-Novoa, C., Lee, C., and Engel, A.: Transparent exopolymer particles (TEP) and
753 Coomassie stainable particles (CSP): Differences between their origin and vertical distributions
754 in the ocean, Marine Chemistry, doi: http://dx.doi.org/10.1016/j.marchem.2015.03.009, 2015.
755 2015.
756 Cunliffe, M., Engel, A., Frka, S., Gašparović , B., Guitart, C., Murrell, J. C., Salter, M., Stolle, C.,
757 Upstill-Goddard, *R*., and Wurl, O.: Sea surface microlayers: A unified physicochemical and
758 biological perspective of the air-ocean interface, Progr. Oceanogr., 109, 104-116, 2013.
759 Cunliffe, M. and Murrell, J. C.: The sea-surface microlayer is a gelatinous biofilm, The ISME
760 journal, 3, 1001-1003, 2009.
761 Cunliffe, M., Upstill-Goddard, *R*. C., and Murrell, J. C.: Microbiology of aquatic surface
762 microlayers, FEMS Microbiol. Rev., 35, 233-246, 2011.
763 Cunliffe, M. and Wurl, O.: Guide to best practices to study the ocean's surface., Plymouth, UK,
764 2014.
765 Davies, J. T.: The Effects of Surface Films in Damping Eddies at a Free Surface of a Turbulent
766 Liquid, 1966.
767 Dickson, A. G., Sabine, C. L., and Christian, J. *R*.: Guide to best practices for ocean CO2
768 measurements, PICES, 2007.
769 Dittmar, T., Cherrier, J., and Ludwichowski, K.-U.: The Analysis of Amino Acids in Seawater. In:
770 Practical Guidelines for the Analysis of Seawater, CRC Press, 2009.
771 Engel, A.: Determination of Marine Gel Particles. In: Practical Guidelines for the Analysis of
772 Seawater, CRC Press, 2009.
773 Engel, A.: The role of transparent exopolymer particles (TEP) in the increase in apparent particle
774 stickiness (α) during the decline of a diatom bloom, Journal of Plankton Research, 22, 485-497,
775 2000.
776 Engel, A., Borchard, C., Loginova, A., Meyer, J., Hauss, H., and Kiko, *R*.: Effects of varied nitrate
777 and phosphate supply on polysaccharidic and proteinaceous gel particles production during
778 tropical phytoplankton bloom experiments, Biogeosciences Discuss., 12, 6589-6635, 2015.
779 Engel, A., Borchard, C., Piontek, J., Schulz, K. G., Riebesell, U., and Bellerby, *R*.: CO2 increases
780 14C primary production in an Arctic plankton community, Biogeosciences, 10, 1291-1308, 2013.
781 Engel, A. and Händel, N.: A novel protocol for determining the concentration and composition of
782 sugars in particulate and in high molecular weight dissolved organic matter (HMW-DOM) in
783 seawater, Marine Chemistry, 127, 180-191, 2011.
784 Engel, A. and Schartau, M.: Influence of transparent exopolymer particles (TEP) on sinking
785 velocity of Nitzschia closterium aggregates, Marine Ecology Progress Series, 182, 69-76, 1999.
786 Engel, A., Thoms, S., Riebesell, U., Rochelle-Newall, E., and Zondervan, I.: Polysaccharide
787 aggregation as a potential sink of marine dissolved organic carbon, Nature, 428, 929-932, 2004.
788 Falkowska, L.: Sea surface microlayer: a field evaluation of teflon plate, glass plate and screen
789 sampling techniques. Part 1. Thickness of microlayer samples and relation to wind speed,
790 Oceanologia, 41, 211-221, 1999.
791 Frew, N. M.: The role of organic films in air-sea gas exchange. In: The Sea Surface and Global
792 Change, Liss, P. S. and Duce, *R*. A. (Eds.), Cambridge University Press, UK, 1997.
793 Frew, N. M., Bock, E. J., Schimpf, U., Hara, T., Haußecker, H., Edson, J. B., McGillis, W. *R*., Nelson,
794 *R*. K., McKenna, S. P., Uz, B. M., and Jähne, B.: Air-sea gas transfer: Its dependence on wind
795 stress, small-scale roughness, and surface films, Journal of Geophysical Research: Oceans, 109,
796 n/a-n/a, 2004.

797 Frew, N. M., Goldman, J. C., Dennett, M. *R*., and Johnson, A. S.: Impact of phytoplankton-
798 generated surfactants on air-sea gas exchange, Journal of Geophysical Research: Oceans, 95,
799 3337-3352, 1990.
800 Fuhrman, J. A. and Ferguson, *R*. L.: Nanomolar concentrations and rapid turnover of dissolved
801 free amino acids in seawater: agreement between chemical and microbiological measurements,
802 Marine Ecology Progress Series, 33, 237-242, 1986.
803 Galgani, L. and Engel, A.: Accumulation of Gel Particles in the Sea-Surface Microlayer during an
804 Experimental Study with the Diatom Thalassiosira weissflogii, International Journal of
805 Geosciences, 4, 129-145, 2013.
806 Galgani, L., Stolle, C., Endres, S., Schulz, K. G., and Engel, A.: Effects of ocean acidification on the
807 biogenic composition of the sea-surface microlayer: Results from a mesocosm study, J.
808 Geophys. Res-Oceans, 119, 7911-7924, 2014.
809 Gao, Q., Leck, C., Rauschenberg, C., and Matrai, P. A.: On the chemical dynamics of extracellular
810 polysaccharides in the high Arctic surface microlayer, Ocean Sci., 8, 401-418, 2012.
811 Garreaud, *R*. D., Rutllant, J. A., Muñoz, *R*. C., Rahn, D. A., Ramos, M., and Figueroa, D.: VOCALS-
812 CUpEx: the Chilean Upwelling Experiment, Atmos. Chem. Phys., 11, 2015-2029, 2011.
813 GESAMP: The Sea-Surface Microlayer and its Role in Global Change. Reports and Studies, WMO,
814 1995.
815 Gutknecht, E., Dadou, I., Marchesiello, P., Cambon, G., Le Vu, B., Sudre, J., Garçon, V., Machu, E.,
816 Rixen, T., Kock, A., Flohr, A., Paulmier, A., and Lavik, G.: Nitrogen transfers off Walvis Bay: a 3-D
817 coupled physical/biogeochemical modeling approach in the Namibian upwelling system,
818 Biogeosciences, 10, 4117-4135, 2013.
819 Harvey, G. W. and Burzell, L. A.: A simple microlayer method for small samples, Limnol.
820 Oceanogr., 11, 608-614, 1972.
821 Hatcher, *R*. F. and Parker, B. C.: Laboratory comparisons of four surface microlayer samplers1,
822 Limnology and Oceanography, 19, 162-165, 1974.
823 Hawkins, L. N., Russell, L. M., Covert, D. S., Quinn, P. K., and Bates, T. S.: Carboxylic acids,
824 sulfates, and organosulfates in processed continental organic aerosol over the southeast Pacific
825 Ocean during VOCALS-REx 2008, Journal of Geophysical Research: Atmospheres, 115, n/a-n/a,
826 2010.
827 Henrichs, S. M. and Williams, P. M.: Dissolved and particulate amino acids and carbohydrates in
828 the sea surface microlayer, Marine Chemistry, 17, 141-163, 1985.
829 Hu, H., Bourbonnais, A., Larkum, J., Bange, H. W., and Altabet, M. A.: Nitrogen cycling in shallow
830 low oxygen coastal waters off Peru from nitrite and nitrate nitrogen and oxygen isotopes,
831 Biogeosciences Discuss., 12, 7257-7299, 2015.
832 Jähne, B. and Haußecker, H.: AIR-WATER GAS EXCHANGE, Annual Review of Fluid Mechanics, 30,
833 443-468, 1998.
834 Keeling, *R*. F., Körtzinger, A., and Gruber, N.: Ocean Deoxygenation in a Warming World, Annu.
835 Rev. Mar. Sci., 2, 199-229, 2010.
836 Keil, *R*. G. and Kirchman, D. L.: Bacterial Hydrolysis of Protein and Methylated Protein and Its
837 Implications for Studies of Protein Degradation in Aquatic Systems, Applied and Environmental
838 Microbiology, 58, 1374-1375, 1992.
839 Kuznetsova, M. and Lee, C.: Dissolved free and combined amino acids in nearshore seawater,
840 sea surface microlayers and foams: Influence of extracellular hydrolysis, Aquatic Sciences -
841 Research Across Boundaries, 64, 252-268, 2002.

842 Kuznetsova, M. and Lee, C.: Enhanced extracellular enzymatic peptide hydrolysis in the sea-
843 surface microlayer, Marine Chemistry, 73, 319-332, 2001.
844 Kuznetsova, M., Lee, C., and Aller, J.: Characterization of the proteinaceous matter in marine
845 aerosols, Marine Chemistry, 96, 359-377, 2005.
846 Kuznetsova, M., Lee, C., and Aller, J.: Enrichment of amino acids in the sea surface microlayer at
847 coastal and open ocean sites in the North Atlantic Ocean, Limnol. Oceanogr., 49, 1605-1619,
848 2004.
849 Lachkar, Z. and Gruber, N.: What controls biological production in coastal upwelling systems?
850 Insights from a comparative modeling study, Biogeosciences, 8, 2961-2976, 2011.
851 Laß, K., Bange, H. W., and Friedrichs, G.: Seasonal signatures in SFG vibrational spectra of the
852 sea surface nanolayer at Boknis Eck Time Series Station (SW Baltic Sea), Biogeosciences, 10,
853 5325-5334, 2013.
854 Leck, C. and Bigg, E. K.: Source and evolution of the marine aerosol—A new perspective,
855 Geophysical Research Letters, 32, L19803, 2005.
856 Lindroth, P. and Mopper, K.: High performance liquid chromatographic determination of
857 subpicomole amounts of amino acids by precolumn fluorescence derivatization with o-
858 phthaldialdehyde, Anal. Chem., 51, 1667-1674, 1979.
859 Liss, P. S.: Gas Transfer: Experiments and Geochemical Implications. In: Air-Sea Exchange of
860 Gases and Particles, Liss, P. and Slinn, W. G. (Eds.), NATO ASI Series, Springer Netherlands, 1983.
861 Liss, P. S. and Duce, *R*. A.: The Sea Surface and Global Change, Cambridge University Press, 2005.
862 Logan, B. E., Passow, U., Alldredge, A. L., Grossartt, H.-P., and Simont, M.: Rapid formation and
863 sedimentation of large aggregates is predictable from coagulation rates (half-lives) of
864 transparent exopolymer particles (TEP), Deep Sea Research Part II: Topical Studies in
865 Oceanography, 42, 203-214, 1995.
866 Long, *R*. A. and Azam, F.: Abundant protein-containing particles in the sea, Aquatic Microbial
867 Ecology, 10, 213-221, 1996.
868 Mari, X. and Burd, A.: Seasonal size spectra of transparent exopolymeric particles (TEP) in a
869 coastal sea and comparison with those predicted using coagulation theory, Marine Ecology
870 Progress Series, 163, 63-76, 1998.
871 Mari, X. and Kiørboe, T.: Abundance, size distribution and bacterial colonization of transparent
872 exopolymeric particles (TEP) during spring in the Kattegat, Journal of Plankton Research, 18,
873 969-986, 1996.
874 Matrai, P. A., Tranvik, L., Leck, C., and Knulst, J. C.: Are high Arctic surface microlayers a
875 potential source of aerosol organic precursors?, Mar. Chem., 108, 109-122, 2008.
876 Meakin, P.: Fractal aggregates in geophysics, Reviews of Geophysics, 29, 317-354, 1991.
877 O'Dowd, C. D., Facchini, M. C., Cavalli, F., Ceburnis, D., Mircea, M., Decesari, S., Fuzzi, S., Yoon, Y.
878 J., and Putaud, J.-P.: Biogenically driven organic contribution to marine aerosol, Nature, 431,
879 676-680, 2004.
880 Orellana, M. V., Matrai, P. A., Leck, C., Rauschenberg, C. D., Lee, A. M., and Coz, E.: Marine
881 microgels as a source of cloud condensation nuclei in the high Arctic, Proceedings of the
882 National Academy of Sciences, 108, 13612-13617, 2011.
883 Panagiotopoulos, C., Sempéré, *R*., Lafont, *R*., and Kerhervé, P.: Sub-ambient temperature effects
884 on the separation of monosaccharides by high-performance anion-exchange chromatography
885 with pulse amperometric detection: Application to marine chemistry, Journal of
886 Chromatography A, 920, 13-22, 2001.

887 Passow, U.: Transparent exopolymer particles (TEP) in aquatic environments, Progress in
888 Oceanography, 55, 287-333, 2002.
889 Paulmier, A. and Ruiz-Pino, D.: Oxygen minimum zones (OMZs) in the modern ocean, Progr.
890 Oceanogr., 80, 113-128, 2009.
891 Paulmier, A., Ruiz-Pino, D., and Garcon, V.: The oxygen minimum zone (OMZ) off Chile as
892 intense source of CO2 and N2O, Cont. Shelf Res. , 28, 2746-2756, 2008.
893 Paulmier, A., Ruiz-Pino, D., and Garçon, V.: CO2 maximum in the oxygen minimum zone (OMZ),
894 Biogeosciences, 8, 239-252, 2011.
895 Prieto, L., Ruiz, J., Echevarría, F., García, C. M., Bartual, A., Gálvez, J. A., Corzo, A., and Macías,
896 D.: Scales and processes in the aggregation of diatom blooms: high time resolution and wide
897 size range records in a mesocosm study, Deep Sea Research Part I: Oceanographic Research
898 Papers, 49, 1233-1253, 2002.
899 Quinn, P. K. and Bates, T. S.: The case against climate regulation via oceanic phytoplankton
900 sulphur emissions, Nature, 480, 51-56, 2011.
901 Quinn, P. K., Bates, T. S., Schulz, K. S., Coffman, D. J., Frossard, A. A., Russell, L. M., Keene, W. C.,
902 and Kieber, D. J.: Contribution of sea surface carbon pool to organic matter enrichment in sea
903 spray aerosol, Nature Geosci, 7, 228-232, 2014.
904 Reinthaler, T., Sintes, E., and Herndl, G. J.: Dissolved organic matter and bacterial production
905 and respiration in the sea-surface microlayer of the open Atlantic and the western
906 Mediterranean Sea, Limnol. Oceanogr., 53, 122-136, 2008.
907 Riebesell, U., Kortzinger, A., and Oschlies, A.: Tipping Elements in Earth Systems Special Feature:
908 Sensitivities of marine carbon fluxes to ocean change, Proceedings of the National Academy of
909 Sciences, 106, 20602-20609, 2009.
910 Russell, L. M., Hawkins, L. N., Frossard, A. A., Quinn, P. K., and Bates, T. S.: Carbohydrate-like
911 composition of submicron atmospheric particles and their production from ocean bubble
912 bursting, Proceedings of the National Academy of Sciences, 107, 6652-6657, 2010.
913 Salter, M. E., Upstill-Goddard, *R*. C., Nightingale, P. D., Archer, S. D., Blomquist, B., Ho, D. T.,
914 Huebert, B., Schlosser, P., and Yang, M.: Impact of an artificial surfactant release on air-sea gas
915 fluxes during Deep Ocean Gas Exchange Experiment II, Journal of Geophysical Research: Oceans,
916 116, C11016, 2011.
917 Santos, A. L., Oliveira, V., Baptista, I., Henriques, I., Gomes, N. C., Almeida, A., Correia, A., and
918 Cunha, A.: Effects of UV-B radiation on the structural and physiological diversity of
919 bacterioneuston and bacterioplankton, Appl. Environ. Microbiol., 78, 2066-2069, 2012.
920 Schlitzer, *R*.: Ocean Data View. 2013.
921 Schulz, K. G., Bellerby, *R*. G. J., Brussaard, C. P. D., Büdenbender, J., Czerny, J., Engel, A., Fischer,
922 M., Koch-Klavsen, S., Krug, S. A., Lischka, S., Ludwig, A., MeyerhѴðfer, M., Nondal, G., Silyakova,
923 A., Stuhr, A., and Riebesell, U.: Temporal biomass dynamics of an Arctic plankton bloom in
924 response to increasing levels of atmospheric carbon dioxide, Biogeosciences, 10, 161-180, 2013.
925 Sieburth, J. M.: Microbiological and organic-chemical processes in the surface and mixed layers -
926 Air-Sea exchange of Gases and Particles, D.Reidel Publishing Company, 1983.
927 Solomon, S., Qin, D., Manning, M., Chen, Z., Marquis, M., Averyt, K. B., Tignor, M., and Miller, H.
928 L.: Climate Change 2007: The Physical Science Basis. Contribution of Working Group I to the
929 Fourth Assessment Report of the Intergovernmental Panel on Climate Change, Cambridge,
930 United Kingdom and New York, NY, USA, Cambridge University Press, 2007.

931 Steinfeldt, *R*., Sültenfuß, J., Dengler, M., Fischer, T., and Rhein, M.: Coastal upwelling off Peru
932 and Mauritania inferred from helium isotope disequilibrium, Biogeosciences Discuss., 12, 11019-
933 11059, 2015.
934 Stolle, C., Nagel, K., Labrenz, M., and Jürgens, K.: Bacterial activity in the sea-surface microlayer:
935 in situ investigations in the Baltic Sea and the influence of sampling devices, Aquatic Microbial
936 Ecology, 58, 67-78, 2009.
937 Stramma, L., Johnson, G. C., Sprintall, J., and Mohrholz, V.: Expanding Oxygen-Minimum Zones
938 in the Tropical Oceans, Science, 320, 655-658, 2008.
939 Sugimura, Y. and Suzuki, Y.: A high-temperature catalytic oxidation method for the
940 determination of non-volatile dissolved organic carbon in seawater by direct injection of a liquid
941 sample, Marine Chemistry, 24, 105-131, 1988.
942 Tarazona, J. and Arntz, W.: The Peruvian Coastal Upwelling System. In: Coastal Marine
943 Ecosystems of Latin America, Seeliger, U. and Kjerfve, B. (Eds.), Ecological Studies, Springer
944 Berlin Heidelberg, 2001.
945 Upstill-Goddard, *R*. C., Frost, T., Henry, G. *R*., Franklin, M., Murrell, J. C., and Owens, N. J. P.:
946 Bacterioneuston control of air-water methane exchange determined with a laboratory gas
947 exchange tank, Global biogeochemical cycles, 17, 1108, 2003.
948 Verdugo, P., Alldredge, A. L., Azam, F., Kirchman, D. L., Passow, U., and Santschi, P. H.: The
949 oceanic gel phase: a bridge in the DOM–POM continuum, Marine Chemistry, 92, 67-85, 2004.
950 Wallace, G. T. and Duce, *R*. A.: Transport of particulate organic matter by bubbles in marine
951 waters 1, Limnology and Oceanography, 23, 1155-1167, 1978.
952 Wilson, T. W., Ladino, L. A., Alpert, P. A., Breckels, M. N., Brooks, I. M., Browse, J., Burrows, S.
953 M., Carslaw, K. S., Huffman, J. A., Judd, C., Kilthau, W. P., Mason, *R*. H., McFiggans, G., Miller, L.
954 A., Najera, J. J., Polishchuk, E., Rae, S., Schiller, C. L., Si, M., Temprado, J. V., Whale, T. F., Wong,
955 J. P. S., Wurl, O., Yakobi-Hancock, J. D., Abbatt, J. P. D., Aller, J. Y., Bertram, A. K., Knopf, D. A.,
956 and Murray, B. J.: A marine biogenic source of atmospheric ice-nucleating particles, Nature, 525,
957 234-238, 2015.
958 Wood, *R*., Mechoso, C. *R*., Bretherton, C. S., Weller, *R*. A., Huebert, B., Straneo, F., Albrecht, B.
959 A., Coe, H., Allen, G., Vaughan, G., Daum, P., Fairall, C., Chand, D., Gallardo Klenner, L.,
960 Garreaud, *R*., Grados, C., Covert, D. S., Bates, T. S., Krejci, *R*., Russell, L. M., de Szoeke, S.,
961 Brewer, A., Yuter, S. E., Springston, S. *R*., Chaigneau, A., Toniazzo, T., Minnis, P., Palikonda, *R*.,
962 Abel, S. J., Brown, W. O. J., Williams, S., Fochesatto, J., Brioude, J., and Bower, K. N.: The VAMOS
963 Ocean-Cloud-Atmosphere-Land Study Regional Experiment (VOCALS-REx): goals, platforms, and
964 field operations, Atmos. Chem. Phys., 11, 627-654, 2011.
965 Wurl, O., Miller, L., Röttgers, *R*., and Vagle, S.: The distribution and fate of surface-active
966 substances in the sea-surface microlayer and water column, Marine Chemistry, 115, 1-9, 2009.
967 Wurl, O., Miller, L., and Vagle, S.: Production and fate of transparent exopolymer particles in the
968 ocean, J. geophys. Res., 116, C00H13, 2011.
969 Yu, H. and Mou, S.-F.: Effect of temperature on the retention of amino acids and carbohydrates
970 in high-performance anion-exchange chromatography, Journal of Chromatography A, 1118, 118-
971 124, 2006.
972 Zhang, Z.: Studies on the sea surface microlayer II. The layer of sudden change of physical and
973 chemical properties, Journal of Colloid and Interface Science, 264, 148-159, 2003.

974 Zhang, Z., Liu, L., Wu, Z., Li, J., and Ding, H.: Physicochemical Studies of the Sea Surface
975 Microlayer: I. Thickness of the Sea Surface Microlayer and Its Experimental Determination, J.
976 Colloid Interface Sci., 204, 294-299, 1998.
977 Zhou, J., Mopper, K., and Passow, U.: The role of surface-active carbohydrates in the formation
978 of transparent exopolymer particles by bubble adsorption of seawater, Limnology and
979 Oceanography, 43, 1860-1871, 1998.
980
981

Legends

Figure 1: Maps of stations where sampling for sea surface microlayer (SML) and underlying seawater (ULW) was conducted during the SOPRAN Meteor 91 cruise along the coastal upwelling area off Peru in 2012.

Figure 2a, b: Surface water (1m depth) temperature (°C) and wind speed (m s^{-1}) (b) during M91.

Figure 3: Direct relationship between surface water temperature and wind speed during M91 SML sampling, $p<0.001$, $r= 0.58$, $n=37$. Data in dotted rectangle were selected for analysis of wind speed effects at similar temperatures, see figure 7.

Figure 4: Phyto- and bacterioneuston (<20 µm) abundance (number mL^{-1}) in the SML off Peru during M93: NCPL: 'Non-cyanobacterial-type' phytoplankton, CPL: 'cyanobacterial-type' phytoplankton, HPL: heterotrophic bacterioplankton.

Figure 5: Surface distribution patterns of organic matter concentrations in the SML during M91 showing particulate organic carbon (POC, µmol L^{-1}), dissolved organic carbon (DOC, µmol L^{-1}) dissolved hydrolysable carbohydrates (DCCHO, nmol L^{-1}), dissolved hydrolysable amino acids (DHAA, nmol L^{-1}) and abundance of TEP (L^{-1}) and CSP (L^{-1}).

Figure 6: Box and whisker plot of enrichment factors (EF) calculated for various particulate and dissolved components during M91. Each box encloses 50% of the data with the median value of the variable displayed as a line. The bottom of the box marks the 25%, and the top the 75% limit, of data. The lines extending from the top and bottom of each box marks the 10% and 90% percentiles within the data set and the filled circles indicate the data outside of this range. For abbreviations, see text.

Figure 7a, b: Influence of wind speed (m s^{-1}) on the total area concentration of TEP (mm^2 L^{-1}) in the SML at all stations (a) and relationship between TEP enrichment factors (EF) and wind speed (m s^{-1}) for only those stations that showed similar sea surface temperature as indicated in figure 3.

Filled dots indicated data from stations of similar sea surface temperature. Data in plot (a) were fitted by power law functions; the solid line represents all data, the dotted line represents data of similar sea surface temperature.

Figure 8a, b: Size frequency distribution of TEP (a) and CSP (b) observed during the M91 cruise for samples collected from the SML (open symbols) and in the ULW (filled symbols) at the stations with lowest wind speed of 0.6 m s^{-1} (triangles) and highest wind speed of 9.0 m s^{-1} (circles). Linear regression of log*(dN/d(dp))* versus log*(dp)* was fitted to the particles in the size range of 1.05 – 14.14 µm ESD.

Figure 9: Spatial distribution of the slope ratio, δ*, for TEP in the upwelling region off Peru during M91.

Tables

Table 1: Hydrographic conditions encountered during SML sampling off Peru in 2012 (M91). Data on air temperature, wind speed, global and UV radiation were obtained from the ship's DShip database for the time of sampling.

	Temperature (°C)	Salinity	Air temperature (°C)	Wind speed ($m\ s^{-1}$)	Global Radiation ($W\ m^{-2}$)	UV Radiation ($W\ m^{-2}$)
average	19.25	34.87	19.67	5.66	570	37935
SD	1.70	0.50	0.89	2.14	366	23384
Min	15.91	32.02	17.30	0.60	10	0.812
Max	21.90	35.32	21.50	9.00	1103	71.10

Table 2: Concentration of various organic components in the SML during M91, given as average (avg.) and standard deviation (SD), as well as minimum (min) and maximum (max); *n* = number of observations. For abbreviations see text.

	Unit	Avg.	SD	min	max	*n*
DOC	µmol L^{-1}	94	13	71	122	39
TOC	µmol L^{-1}	127	33	82	199	39
POC	µmol L^{-1}	33	25	2.3	96	39
TEP number	$x10^6$ L^{-1}	19	15	1.8	63	39
TEP area	mm^2 L^{-1}	100	106	6.9	408	39
DCCHO	nmol L^{-1}	1111	550	507	2668	39
PCCHO	nmol L^{-1}	1084	1300	41	5156	34
TN	µmol L^{-1}	16	4.9	8.7	28	39
TDN	µmol L^{-1}	12.5	4.0	7.7	25	39
PN	µmol L^{-1}	3.3	3.7	bd	16	39
CSP number	$x10^6$ L^{-1}	118	72	19	311	39
CSP area	mm^2 L^{-1}	1024	728	137	3051	39
FAA	nmol L^{-1}	151	104	49	531	37
DHAA	nmol L^{-1}	770	359	423	2017	30
PHAA	nmol L^{-1}	1176	774	208	3956	29
NCPL	$x10^3$ mL^{-1}	45	53	5.4	300	35
CPL	$x10^3$ mL^{-1}	27	35	3.7	193	35
Het. bacteria	$x10^4$ mL^{-1}	195	206	3	854	36

Table 3: Correlation coefficients (*r*) between concentrations of various organic components in the SML and their concentration in the underlying seawater (ULW), temperature (T, °C), and wind speed (U, m s^{-1}) at the time of sampling. Correlations yielding significance level of $p<0.01$ are marked bold. For abbreviations see text. *: only 30 samples were analyzed for NCPL and CPL from the ULW.

SML	r_{ULW}	r_T	r_U	*n*
DOC	**0.75**	-0.04	0.06	39
TOC	**0.79**	**-0.53**	-0.35	39
POC	**0.68**	**-0.67**	**-0.48**	39
TEP number	**0.51**	**-0.58**	**-0.69**	**39**
TEP area	**0.58**	**-0.65**	**-0.69**	**39**
DCCHO	**0.94**	**-0.44**	-0.29	39
PCCHO	**0.77**	**-0.59**	**-0.38**	34
TDN	0.24	-0.18	-0.05	39
PN	**0.59**	**-0.55**	**-0.43**	**39**
CSP number	**0.53**	-0.04	0.15	39
CSP area	**0.68**	-0.36	-0.31	39
FAA	0.34	-0.34	0.19	37
DHAA	0.30	**-0.47**	-0.37	30
PHAA	**0.56**	**-0.64**	**-0.53**	**29**
NCPL	**0.70***	-0,24	-0,21	35
CPL	**0.90***	-0,21	-0,31	35
Het. bacteria	**0.92**	-0.33	**-0.37**	36

Figures

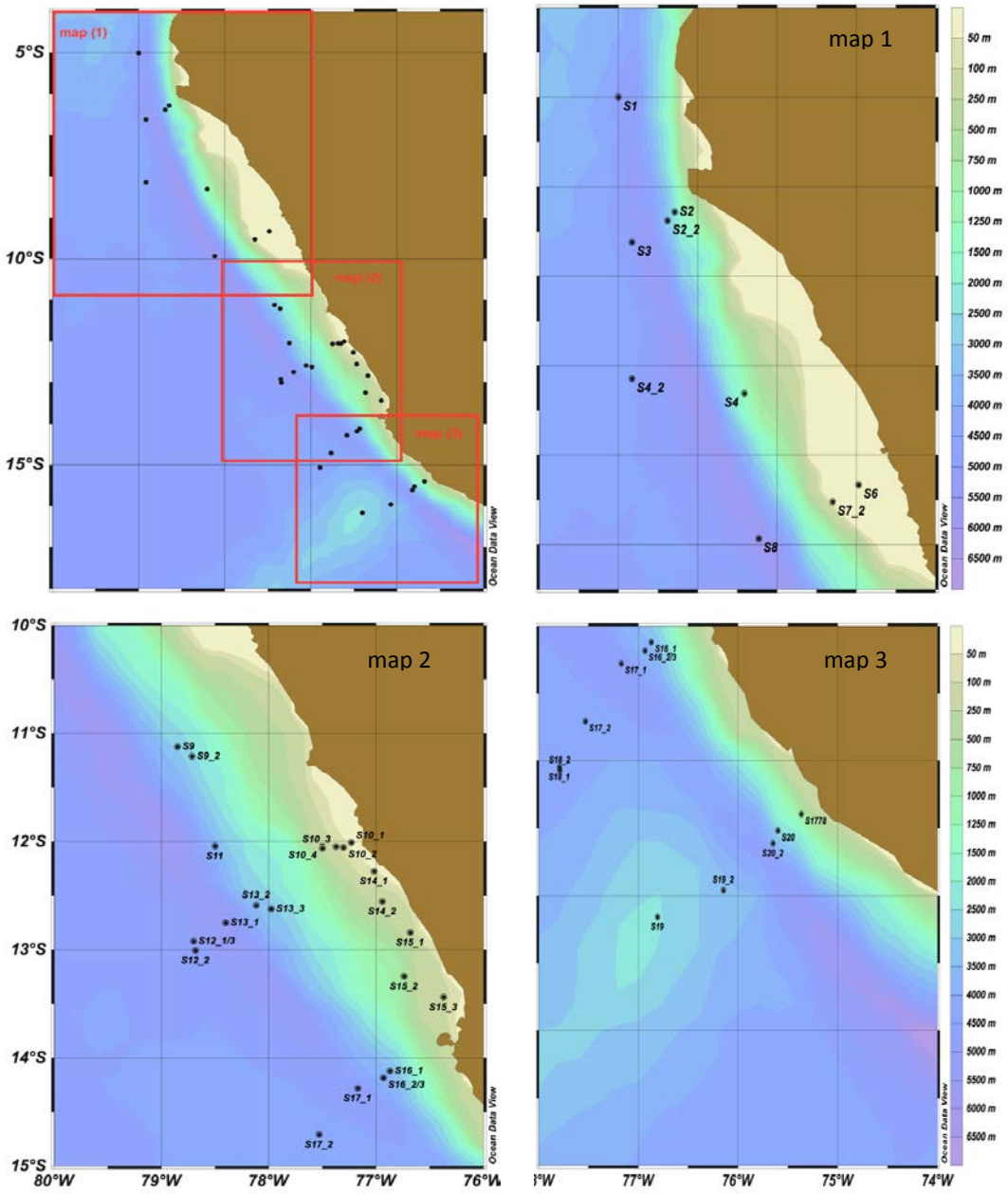

Figure 1

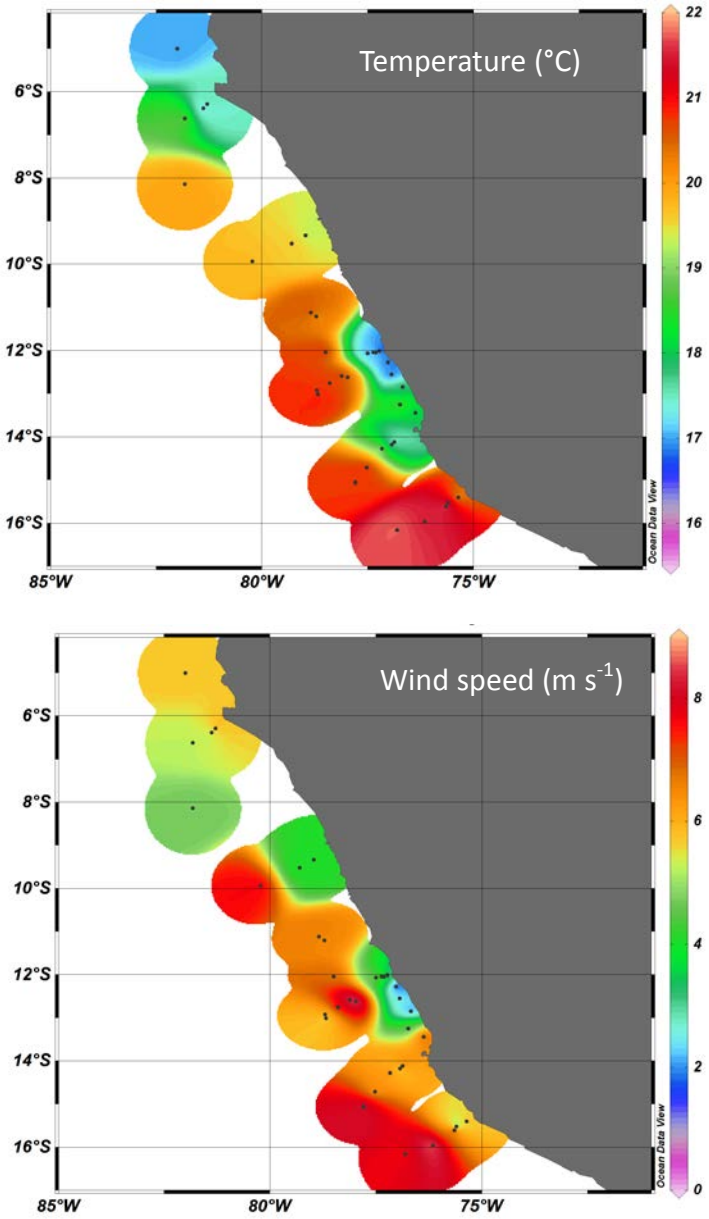
Temperature (°C)
22
21
20
19
18
17
16
6°S
8°S
10°S
12°S
14°S
16°S
85°W
80°W
75°W
Ocean Data View
Wind speed (m s-1)
8
6
4
2
0
6°S
8°S
10°S
12°S
14°S
16°S
85°W
80°W
75°W
Ocean Data View

Figure 2

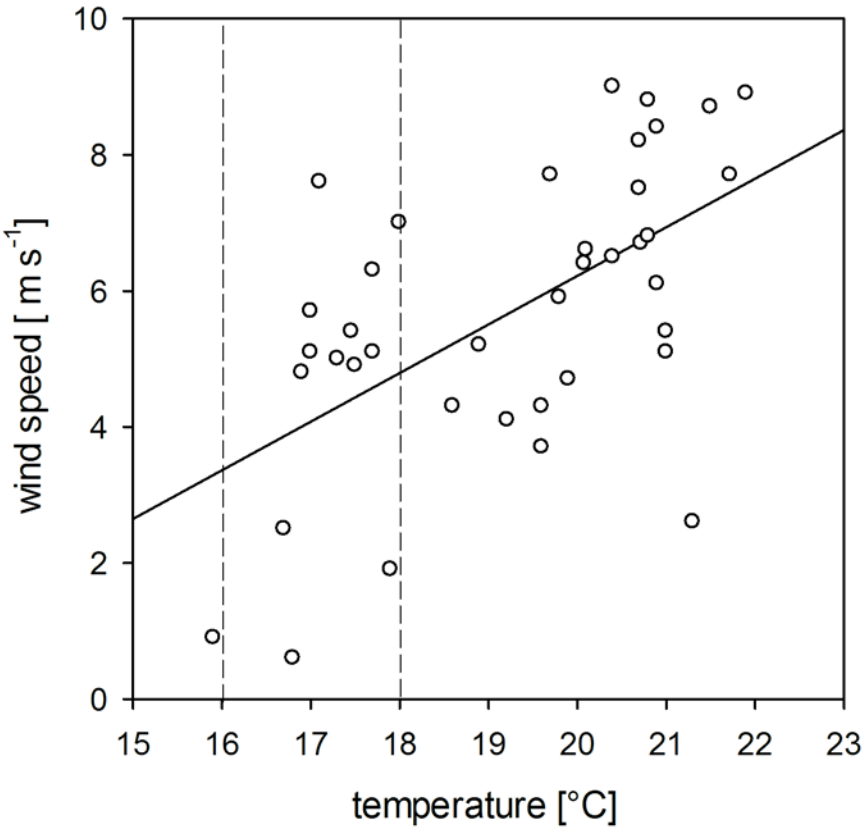

Figure 3

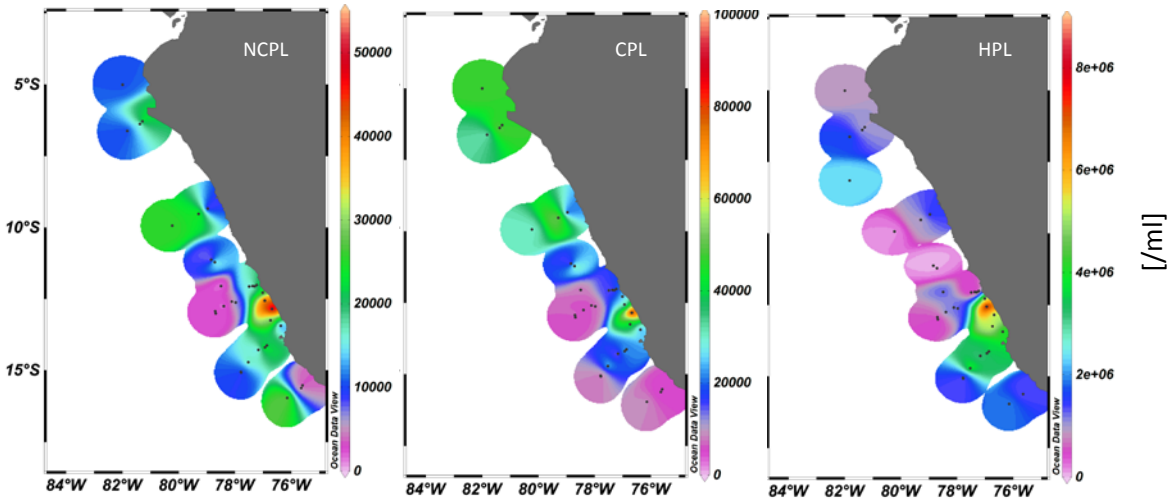

Figure 4

Figure 4

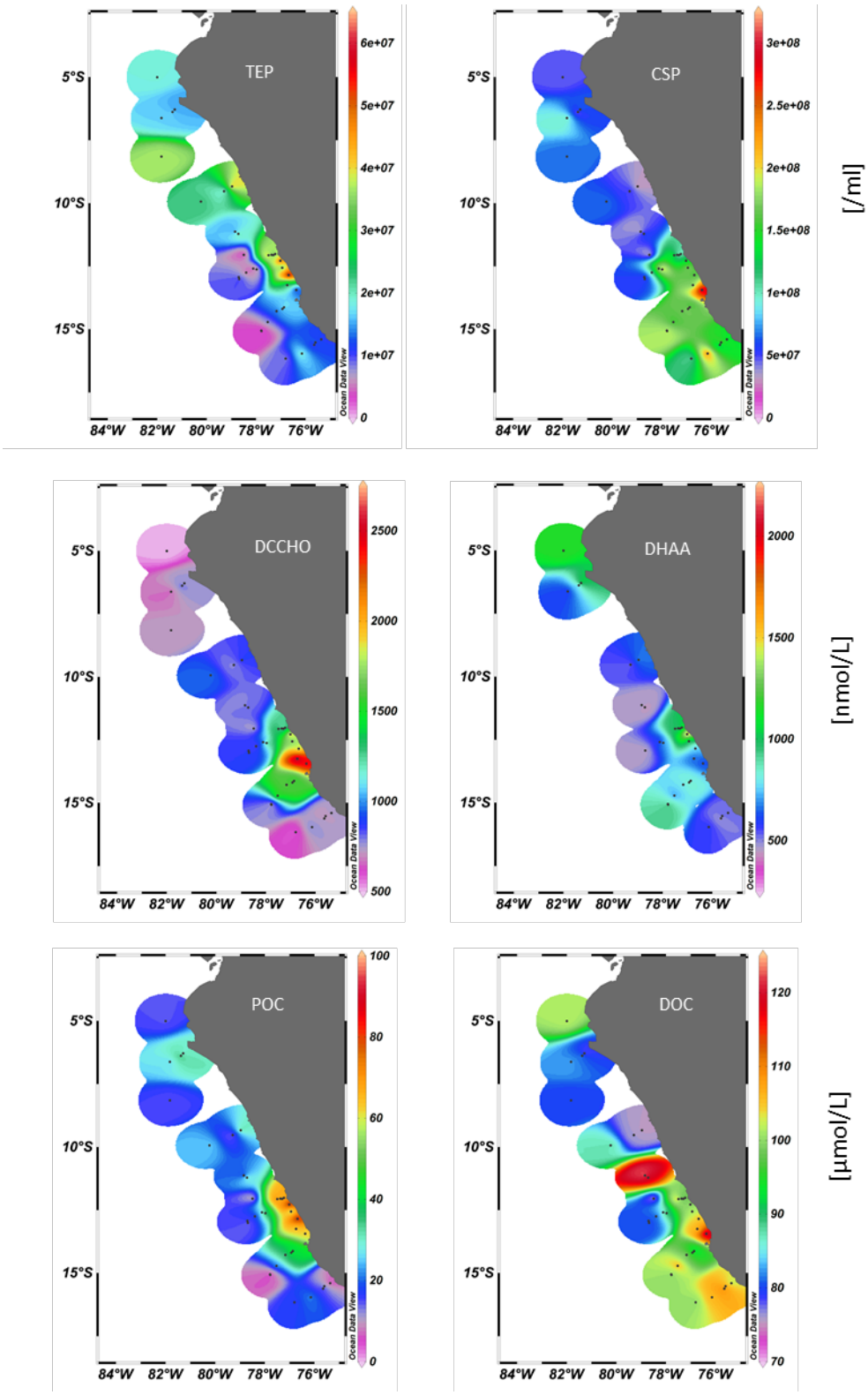
TEP
CSP
DCCHO
DHAA
POC
DOC
5°S
10°S
15°S
84°W
82°W
80°W
78°W
76°W
Ocean Data View
6e+07
5e+07
4e+07
3e+07
2e+07
1e+07
0
3e+08
2.5e+08
2e+08
1.5e+08
1e+08
5e+07
2500
2000
1500
1000
500
100
80
60
40
20
120
110
90
70
[/ml]
[nmol/L]
[µmol/L]

Figure 5

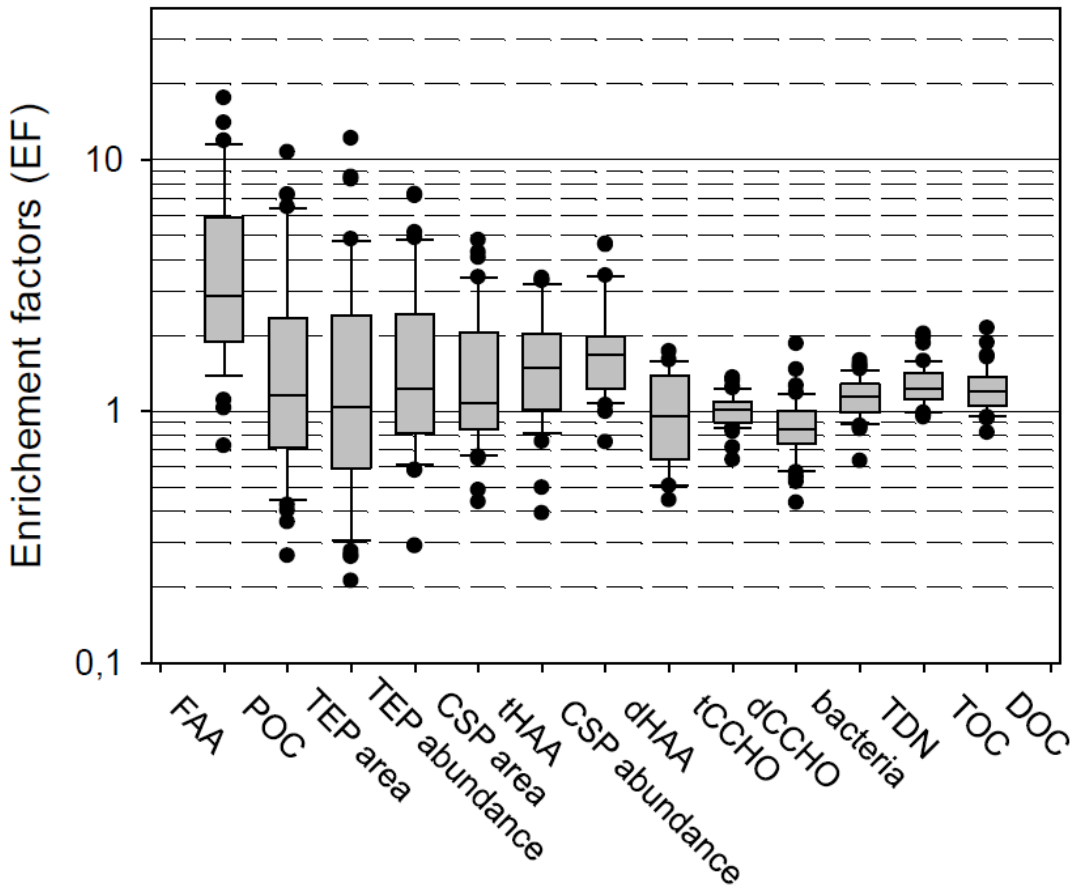
Enrichement factors (EF)
10
1
0,1
FAA
POC
TEP area
TEP abundance
CSP area
tHAA
CSP abundance
dHAA
tCCHO
dCCHO
bacteria
TDN
TOC
DOC

Figure 6

1256

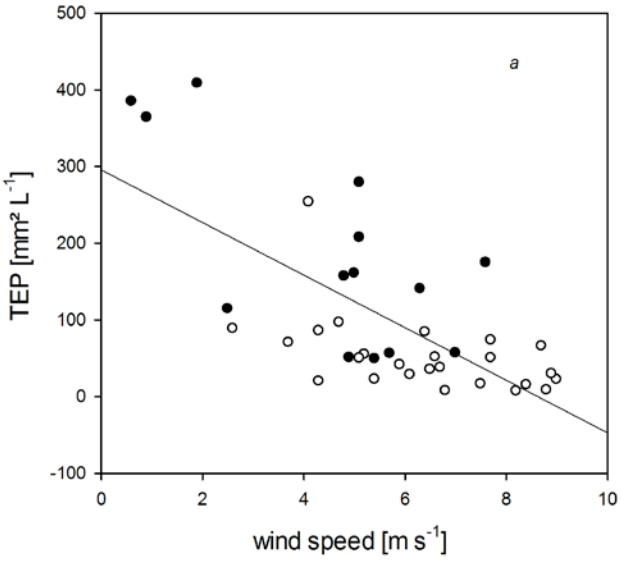

1257

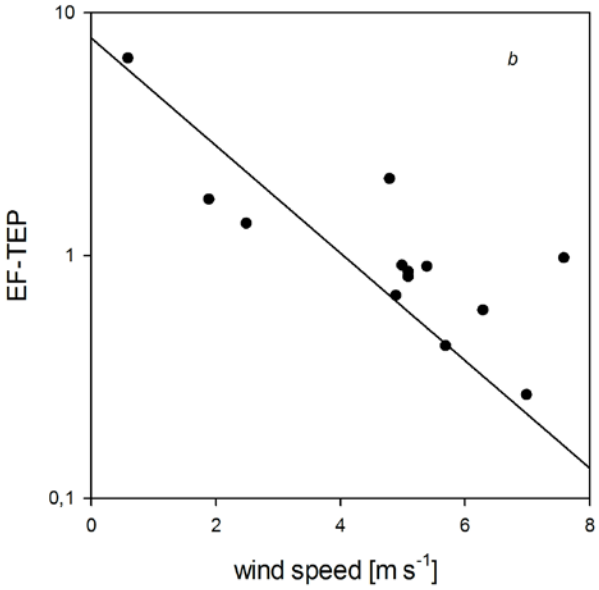

1258

1259 Figure 7a, b

1260

1261

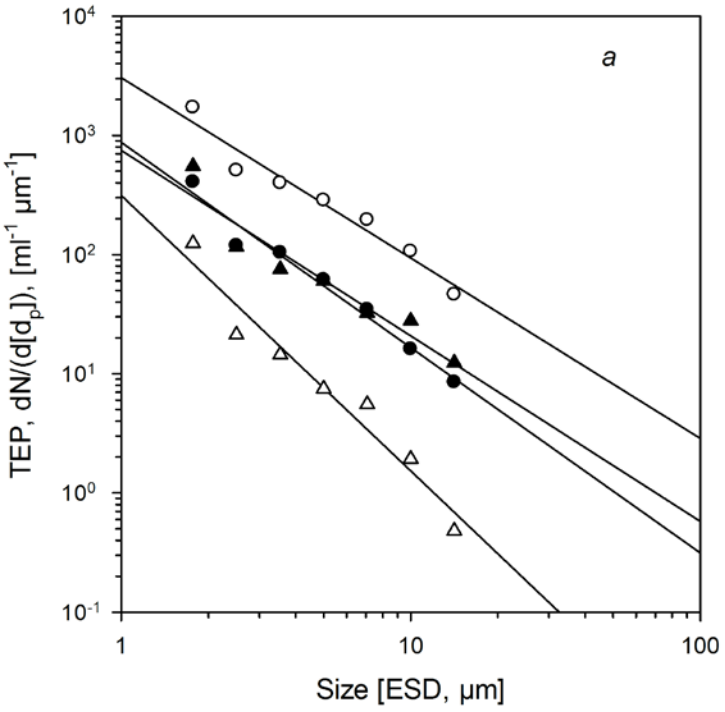

1262

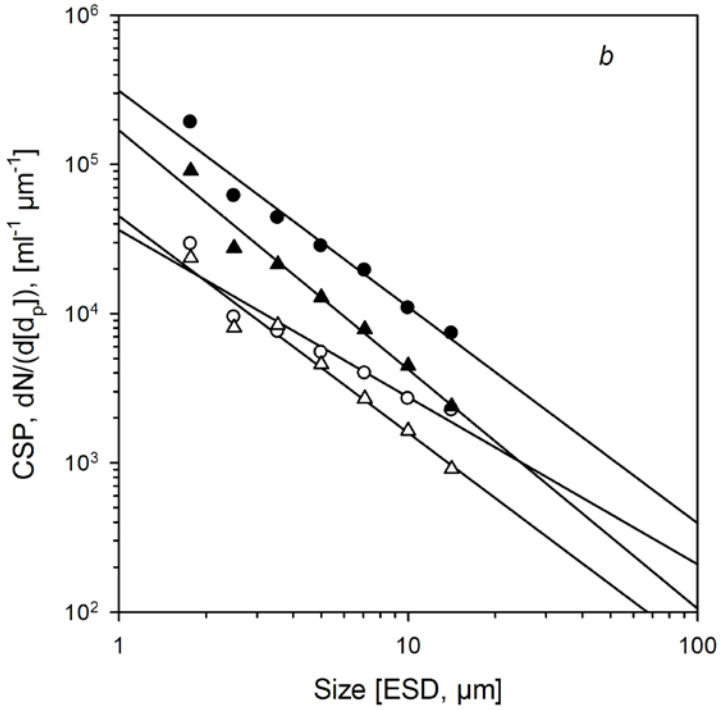

1263

1264

1265 Figure 8a, b

1266

1267

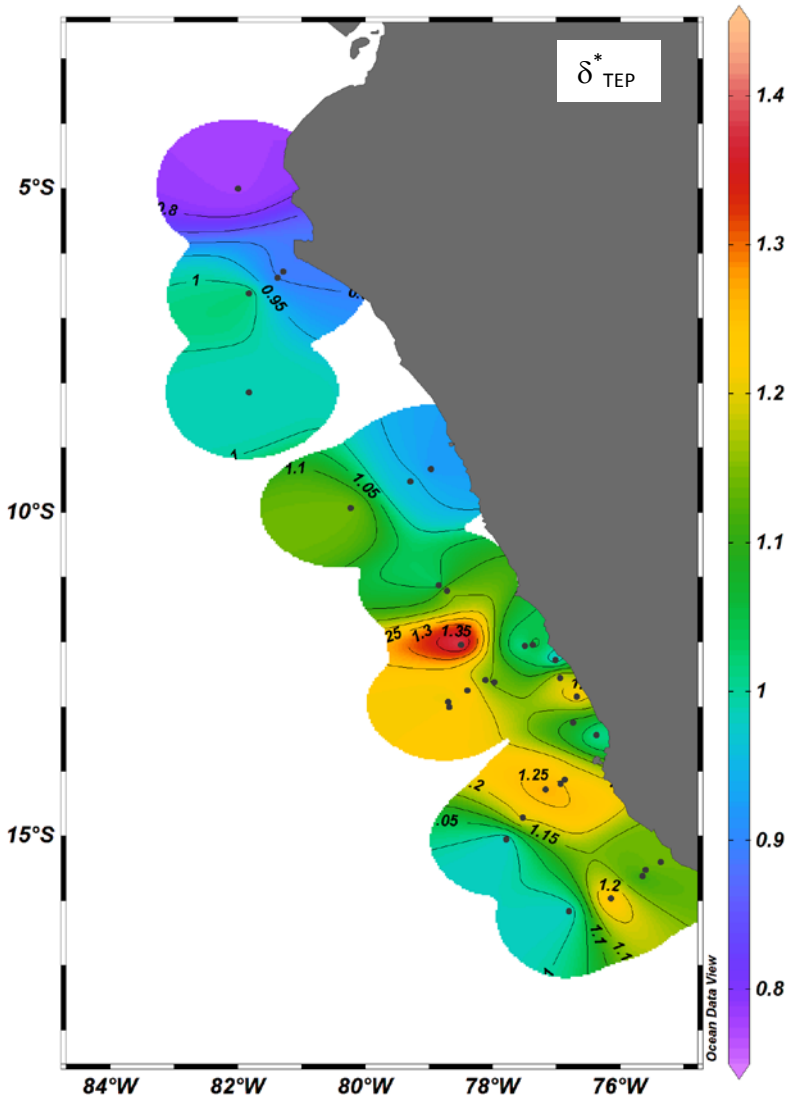
δ* TEP
1.4
1.3
1.2
1.1
1
0.9
0.8
5°S
10°S
15°S
84°W
82°W
80°W
78°W
76°W
Ocean Data View

Figure 9